

Gradient-flow SDEs have unique transient population dynamics

Vincent Guan

University of British Columbia

Joseph Janssen

University of British Columbia

Nicolas Lanzetti

ETH Zürich

Antonio Terpin

ETH Zürich

Geoffrey Schiebinger

University of British Columbia

Elina Robeva

University of British Columbia

Abstract

Identifying the drift and diffusion of an SDE from its population dynamics is a notoriously challenging task. Researchers in machine learning and single cell biology have only been able to prove a partial identifiability result: for potential-driven SDEs, the gradient-flow drift can be identified from temporal marginals if the Brownian diffusivity is already known. Existing methods therefore assume that the diffusivity is known a priori, despite it being unknown in practice. We dispel the need for this assumption by providing a complete characterization of identifiability: the gradient-flow drift and Brownian diffusivity are jointly identifiable from temporal marginals if and only if the process is observed outside of equilibrium. Given this fundamental result, we propose **nn-APPEX**, the first Schrödinger Bridge-based inference method that can simultaneously learn the drift and diffusion of gradient-flow SDEs solely from observed marginals. Extensive numerical experiments show that **nn-APPEX**'s ability to adjust its diffusion estimate enables accurate inference, while previous Schrödinger Bridge methods obtain biased drift estimates due to their assumed, and likely incorrect, diffusion.

1 Introduction

Mathematical biologists conceptualize the evolving genetic profiles of cells, or *developmental trajectories*, with Waddington's epigenetic landscape, which likens differentiating cells to marbles rolling along a surface [Waddington, 1935]. Cell development is therefore thought to be driven by the gradient of this unknown landscape. More broadly, gradient-driven dynamics describe a host of real-world processes, such as contaminant flow within groundwater systems, electric current

within an electromagnetic field, and molecular dynamics driven by interatomic potential energy. Since these processes exhibit stochasticity, they are often modeled by *gradient-flow* SDEs, such that the drift is given by $-\nabla\Psi(X_t)$, and stochasticity is introduced by Brownian motion W_t , with diffusivity $\sigma^2 > 0$ [Weinreb et al., 2018, Lavenant et al., 2024, Lelievre and Stoltz, 2016, Yeo et al., 2021]:

$$dX_t = -\nabla\Psi(X_t)dt + \sigma dW_t. \quad (1)$$

While an SDE's drift and diffusion can generally be inferred from trajectories [Nielsen et al., 2000, Bishwal, 2007, Browning et al., 2020, Wang et al., 2024], it is often only possible to observe population dynamics. For example, hydrogeochemical sensors can only detect plumes, rather than particle trajectories, and scRNA sequencing technologies destroy cells upon measurement [Trapnell et al., 2014]. This limits observations to temporal snapshots of the marginals $(p(\cdot, t))_{t \in [0, T]}$, and raises the fundamental question:

Q: Under what conditions are $-\nabla\Psi$ and σ^2 identifiable from marginals $(p(\cdot, t))_{t \in [0, T]}$?

Despite receiving significant attention from researchers in mathematical biology and machine learning [Hashimoto et al., 2016, Weinreb et al., 2018, Neklyudov et al., 2023, Lavenant et al., 2024, Yeo et al., 2021, Zhang et al., 2021, Chizat et al., 2022, Bunne et al., 2022, Shen et al., 2025, Zhang, 2024, Guan et al., 2024, Terpin et al., 2024, Persiianov et al., 2025], the most comprehensive identifiability results only prove that the drift $-\nabla\Psi$ can be identified from $(p(\cdot, t))_{t \in [0, T]}$ if the diffusivity σ^2 is already known:

observe $(p(\cdot, t))_{t \in [0, T]}$ and σ^2 is known
 $\implies -\nabla\Psi$ is identifiable. (2)

This result, popularized in the mathematical biology community by Weinreb et al. [2018] and in the machine learning community by Hashimoto et al. [2016],

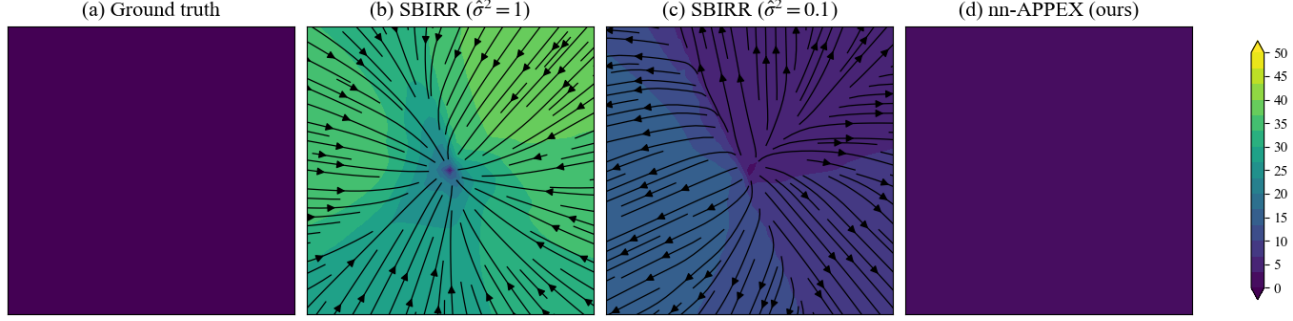


Figure 1: The true drift field (a) and estimated drift fields (b)-(d) are shown for the simple example of a Brownian motion, $dX_t = \sqrt{0.2}dW_t$. The current state-of-the-art Schrödinger Bridge method **SBIRR** [Shen et al., 2025, Zhang, 2024] presumes prior knowledge ($\hat{\sigma}^2$) of the diffusivity σ^2 instead of inferring it from data. Figure 1(b) shows that it may wrongly infer a compressive drift force if $\hat{\sigma}^2 > \sigma^2$, while Figure 1(c) shows that it may wrongly infer an expanding drift force if $\hat{\sigma}^2 < \sigma^2$. Figure 1(d) shows that by iteratively learning the diffusion as well as the drift, our method **nn-APPEX** can accurately infer drift without knowing diffusion a priori.

has informed the predominant view that the only way to achieve principled inference is to assume that the diffusion is already known. As a result of this theory, virtually all inference methods have been developed to estimate $-\nabla\Psi$ given a known diffusivity σ^2 [Hashimoto et al., 2016, Neklyudov et al., 2023, Lavenant et al., 2024, Yeo et al., 2021, Zhang et al., 2021, Chizat et al., 2022, Bunne et al., 2022, Shen et al., 2025, Zhang, 2024]. While the drift is often the principal object of interest, the diffusion is also typically unknown, and contains important insights in its own right, such as the sensitivity of cell fates to initial conditions [Forrow, 2024]. Perhaps most importantly, misspecified diffusion can significantly bias drift estimation. We provide a simple example in Fig. 1, where the true landscape is flat, but overestimated diffusion introduces a sink and underestimated diffusion introduces a source.

Contributions. It has remained an open question whether it is possible and, if so, under which circumstances, *both* the drift and diffusion of a gradient-flow SDE (1) can be identified from its marginals. Our first theoretical contribution is a complete solution to this problem. Theorem 4.2 provides the *necessary and sufficient conditions* for identifying the gradient flow drift and diffusivity from marginals:

$$\begin{aligned} & \text{observe non-stationary } (p(\cdot, t))_{t \in [0, T]} \\ \iff & -\nabla\Psi \text{ and } \sigma^2 \text{ are identifiable.} \end{aligned} \quad (3)$$

We also extend this result beyond the setting of continuous observation $t \in [0, T]$, by proving in Theorem 4.3 that observing three distinct marginals identifies the true SDE from any countable set of candidates, with probability 1. Since our identifiability conditions are commonly observed in practice, our results provide:

1. A theoretical foundation for jointly inferring drift and diffusion directly from marginals.
2. A call to action to move beyond the conventional wisdom that diffusion should be specified a priori for principled inference from population dynamics.

With our identifiability theory guaranteeing that joint inference is well-posed, we propose **nn-APPEX**, the first Schrödinger Bridge (SB) based method capable of estimating both the gradient flow drift $-\nabla\Psi$ and the diffusivity σ^2 . In particular, **nn-APPEX** introduces a diffusion estimation step at each iteration while utilizing neural networks to flexibly infer the drift field. To assess the importance of **nn-APPEX**'s diffusion estimation step, we compare its performance against previous SB methods on popular benchmarks [Terpin et al., 2024, Persianov et al., 2025]. The results corroborate our theory in more practical settings, while also highlighting the importance of learning the correct diffusion for accurate drift estimation, as **nn-APPEX** markedly outperforms previous SB methods.

2 Related works

Our work contributes novel theory and methodology for identifying the true SDE from observed marginals. We overview relevant literature below.

Identifiability theory for population dynamics. To the best of our knowledge, conditions for jointly identifying an SDE's drift and diffusion from marginals have only been proven for linear additive noise SDEs [Guan et al., 2024], which cannot capture the multi-stable dynamics of cell differentiation. For the identifiability of gradient-flow SDEs, the partial identifiability result (2) was first proven by Hashimoto et al. [2016].

Lavenant et al. [2024] extended the result for time-inhomogeneous drift $-\nabla\Psi(x, t)$, and showed that a single sample per marginal suffices, if the measurement times are dense. Finally, Neklyudov et al. [2023] proved that the result also holds if the known diffusivity $\sigma(t)^2$ is time-inhomogeneous.

Schrödinger Bridge based inference methods for population dynamics. A popular approach for marginals-based inference is to reconstruct trajectories with entropic optimal transport, which is equivalent to solving a Schrödinger Bridge (SB) problem [Peyré et al., 2019, Prop. 4.2]. The first such method was Waddington-OT (WOT) [Schiebinger et al., 2019], which performs trajectory inference by solving a single SB problem with respect to a Brownian motion reference with a prescribed diffusivity σ^2 . WOT spawned many variations, which incorporate additional information, like cell lineages [Forrow and Schiebinger, 2021, Venstre et al., 2023], or improve robustness given limited samples [Zhang et al., 2021, Lavenant et al., 2024, Chizat et al., 2022]. In the last year, SB methods were improved with the introduction of iterative reference refinement, i.e. SBIRR [Shen et al., 2025, Zhang, 2024]. Rather than fixing Brownian motion as a reference, SBIRR fixes the diffusivity σ^2 and iteratively re-estimates the drift of the reference process. In contrast to SBIRR, the method that we introduce in this work, nn-APPEX, additionally re-estimates the diffusivity at each iteration. nn-APPEX builds upon the tri-level iterative scheme of APPEX [Guan et al., 2024], which was specifically developed for linear additive noise SDEs, by using a neural network to estimate the nonlinear drift fields encountered in gradient-flow SDEs.

Other inference methods for population dynamics. In addition to SB methods, variational energy-based methods [Hashimoto et al., 2016, Bunne et al., 2022, Neklyudov et al., 2023, Terpin et al., 2024, Persianov et al., 2025] have been developed for SDE inference from population dynamics. These methods leverage the fact that the marginals of potential-driven SDEs minimize a corresponding energy, and use discrete numerical schemes to approximate the underlying parameters. Of these, only JKOnet* [Terpin et al., 2024], jointly estimates drift and diffusion. However, their work did not study identifiability theory, and therefore lacked guarantees for principled inference. We perform experiments comparing the performance of nn-APPEX and JKOnet* in the Supplement. We also note that recent work presents another framework for joint inference via maximum mean discrepancy minimization [Berlinghieri et al., 2025].

3 Mathematical background

As is standard in stochastic analysis [Guan et al., 2024, Shen et al., 2025, Berlinghieri et al., 2025], we ensure that the gradient-flow SDE (1) is well-defined by assuming that the drift $-\nabla\Psi$ satisfies Lipschitz continuity and linear growth, $\|\nabla\Psi(x)\| \leq K(1 + \|x\|)$ for some $K > 0$ [Oksendal, 2013, Theorem 5.5]. Given these conditions, and an initial distribution $p(\cdot, 0)$ with finite second moments, the population dynamics are defined by the Fokker-Planck equation. For all $x \in \mathbb{R}^d, t \geq 0$,

$$\begin{aligned} \frac{\partial p(x, t)}{\partial t} &= \mathcal{L}_{-\nabla\Psi, \sigma^2}^*(p(\cdot, t))(x) \\ &:= \nabla \cdot (p(x, t) \nabla\Psi(x)) + \frac{\sigma^2}{2} \Delta p(x, t). \end{aligned} \quad (4)$$

While the Fokker-Planck equation (4) may not be defined pointwise if the arguments are not sufficiently smooth, it can be defined in the weak distributional sense, such that $\mathcal{L}_{-\nabla\Psi, \sigma^2}^*$ is an operator on probability distributions (see Section A.1). We therefore adopt the weak formulation and use standard notation by omitting x [Bogachev et al., 2022], e.g. $\mathcal{L}_{-\nabla\Psi, \sigma^2}^*(p(\cdot, t))$ rather than $\mathcal{L}_{-\nabla\Psi, \sigma^2}^*(p(\cdot, t))(x)$.

We now rigorously define identifiability of gradient-flow SDEs, given continuous observation of their marginals. Intuitively, an SDE with parameters $(-\nabla\Psi_1, \sigma_1^2)$ is identifiable from its marginals if and only if no other SDE, with distinct parameters $(-\nabla\Psi_2, \sigma_2^2) \neq (-\nabla\Psi_1, \sigma_1^2)$, can produce the same probability flow $\frac{\partial p}{\partial t}$.

Definition 3.1 (Identifiability). *The SDE (1) with parameters $(-\nabla\Psi_1, \sigma_1^2)$ is identifiable from its marginals $(p(\cdot, t))_{t \in [0, T]}$ if and only if, $\forall (-\nabla\Psi_2, \sigma_2^2)$,*

$$\begin{aligned} \mathcal{L}_{-\nabla\Psi_1, \sigma_1^2}^*(p(\cdot, t)) &= \mathcal{L}_{-\nabla\Psi_2, \sigma_2^2}^*(p(\cdot, t)) \quad \forall t \in [0, T] \\ \implies (-\nabla\Psi_1, \sigma_1^2) &= (-\nabla\Psi_2, \sigma_2^2), \end{aligned}$$

where the first equality holds in the distributional sense and the second equality holds pointwise in $\mathbb{R}^d \times \mathbb{R}^+$.

The following example [Lavenant et al., 2024, Guan et al., 2024] shows that gradient-flow SDEs (1) are not always identifiable from their marginals $(p(\cdot, t))_{t \in [0, T]}$.

Example 3.2 (Non-identifiability at the stationary distribution). *Consider two SDEs with quadratic potential, i.e. Ornstein-Uhlenbeck processes,*

$$dX_t = -X_t dt + dW_t \quad X_0 \sim p_0 \quad (5)$$

$$dY_t = -10Y_t dt + \sqrt{10}dW_t \quad Y_0 \sim p_0, \quad (6)$$

with $p_0 = \mathcal{N}(0, \frac{1}{2})$, i.e., Gaussian with mean 0 and variance $\frac{1}{2}$. Since p_0 is the stationary distribution for both SDEs, then $X_t, Y_t \sim p(\cdot, t) = p_0$ for all $t \geq 0$, which makes the SDEs non-identifiable from marginals.

4 Identifiability results

In this section, we present our main result in Theorem 4.2, which states that the gradient-flow SDE (1) is identifiable from its marginals, $(p(\cdot, t))_{t \in [0, T]}$, if and only if it is observed outside of equilibrium. We then show in Theorem 4.3 that three distinct marginals identify the true SDE with probability 1 from any countable set of candidate SDEs.

We first prove that non-stationarity is a necessary condition for identifiability, by extending Theorem 3.2 for arbitrary potentials.

Proposition 4.1. *If p_{eq} is a stationary distribution for the SDE (1), then it is also a stationary distribution for the “rescaled” SDE*

$$dX_t = -\alpha \nabla \Psi(X_t) dt + \sqrt{\alpha} \sigma dW_t, \quad (7)$$

for any $\alpha > 0$.

Proof. If p_{eq} is stationary for $\mathcal{L}_{-\nabla \Psi, \sigma^2}^*$, then

$$\begin{aligned} 0 &= \mathcal{L}_{-\nabla \Psi, \sigma^2}^*(p_{\text{eq}}) \\ &= \nabla \cdot (p_{\text{eq}} \nabla \Psi) + \frac{\sigma^2}{2} \Delta p_{\text{eq}} \\ \Leftrightarrow 0 &= \alpha \left(\nabla \cdot (p_{\text{eq}} \nabla \Psi) + \frac{\sigma^2}{2} \Delta p_{\text{eq}} \right) \\ &= \nabla \cdot (p_{\text{eq}} \nabla (\alpha \Psi)) + \frac{(\sqrt{\alpha} \sigma)^2}{2} \Delta p_{\text{eq}} \\ &= \mathcal{L}_{-\nabla(\alpha \Psi), \alpha \sigma^2}^*(p_{\text{eq}}). \end{aligned}$$

Thus, given the initialization $p(\cdot, 0) = p_{\text{eq}}$, we would observe $p(\cdot, t) = p_{\text{eq}} \forall t \geq 0$ for both processes. \square

This shows that the SDE (1) is non-identifiable from its marginals $(p(\cdot, t))_{t \in [0, T]}$ if we observe complete stationarity, $p(\cdot, t) = p(\cdot, 0) \forall t \geq 0$. We now prove that this is the only source of non-identifiability.

Theorem 4.2 (Identifiability of gradient-flow SDEs). *The SDE (1) is non-identifiable from its marginals $(p(\cdot, t))_{t \in [0, T]}$ if and only if $p(\cdot, t) = p(\cdot, 0) \forall t \geq 0$.*

Proof. Theorem 4.1 proves that if $p(\cdot, t) = p(\cdot, 0) \forall t \geq 0$ then the SDE is non-identifiable.

Now, we prove that non-identifiability implies that $p(\cdot, t) = p(\cdot, 0) \forall t \geq 0$. Suppose that SDEs with parameters $(-\nabla \Psi_1, \sigma_1^2)$ and $(-\nabla \Psi_2, \sigma_2^2)$ produce the same marginals $(p(\cdot, t))_{t \in [0, T]}$. Without loss of generality, we may assume that $\sigma_1^2 > \sigma_2^2$, because the previous partial result (2) states if $\sigma_1^2 = \sigma_2^2$, then $\nabla \Psi_1 = \nabla \Psi_2$ also follows [Lavenant et al., 2024, Theorem 2.1]. Then, from Theorem 3.1, for all observed marginals $p(\cdot, t)$,

$$\mathcal{L}_{-\nabla \Psi_1, \sigma_1^2}^*(p(\cdot, t)) = \mathcal{L}_{-\nabla \Psi_2, \sigma_2^2}^*(p(\cdot, t)). \quad (8)$$

By the linearity of the Fokker-Planck operator, we have

$$0 = (\mathcal{L}_{-\nabla \Psi_1, \sigma_1^2}^* - \mathcal{L}_{-\nabla \Psi_2, \sigma_2^2}^*)(p(\cdot, t)) \quad (9)$$

$$= \nabla \cdot (p(\cdot, t) \nabla (\Psi_1 - \Psi_2)) + \frac{\sigma_1^2 - \sigma_2^2}{2} \Delta p(\cdot, t). \quad (10)$$

We note that the PDE (10) is the Fokker-Planck equation, parametrized by the “residual” drift and diffusion. Then, to prove that $p(\cdot, t) = p(\cdot, 0) \forall t \geq 0$, it suffices to show that there is at most one probability distribution, $p(\cdot, t) = \mu$, which solves (10), since each marginal would then coincide. Since the residual diffusivity $\sigma_1^2 - \sigma_2^2 > 0$ is nondegenerate, and the residual drift $-\nabla(\Psi_1 - \Psi_2)$ is Lipschitz and obeys linear growth, it follows that the residual Fokker-Planck equation (10) has at most one stationary distribution [Bogachev et al., 2022, Theorem 4.16, Example 4.1.8]. \square

By reducing non-identifiability to the uniqueness of solutions to an elliptic PDE, our proof provides a fundamental insight about gradient-flow SDEs: *observing non-identifiability between two processes is equivalent to observing a residual process at equilibrium*. If the SDE parameters are time-homogeneous, then each marginal $p(\cdot, t)$ coincides with the unique stationary distribution. Even if the parameters are time-inhomogeneous, non-identifiability is still characterized by equilibrium. However, equilibrium would not imply a static set of marginals, since equilibrium itself may change over time. We provide an example in Theorem B.3, where the stationary distributions of the residual process coincide with Brownian marginals $\mathcal{N}(0, t)$. In Section B, we also prove sufficient conditions for identifiability in the time-inhomogeneous case, when the SDE parameters change at discrete times, a setting commonly observed in cell development [Monnier et al., 2012].

While Theorem 4.1 shows that either the diffusivity σ^2 or the potential Ψ needs to be known to disambiguate the true SDE from other SDEs with the same stationary distribution, Theorem 4.2 shows that this assumption is not required if the marginals are transient. This is important for real-world inference since the condition $p(\cdot, t) = p(\cdot, 0) \forall t \geq 0$ is easily testable, and it is much more common to observe transient behaviour than it is to know an accurate estimate of diffusivity a priori [Forrow, 2024]. However, Theorem 4.2 still relies on continuous observation, while we only observe a finite number of marginals in practice. We address this by showing that observing three distinct marginals is enough to identify the true SDE from any countable set of candidates, e.g. the set of SDEs that can be represented on a computer. To facilitate the proof, we assume that $\Psi \in C^\infty(\mathbb{R}^d)$ for this result (see details in Section A.2).

Corollary 4.3 (Identifiability from three marginals). *Let \mathcal{S} be a countable set of gradient-flow SDEs with*

smooth potentials, which all share the same initial distribution $p(\cdot, 0)$. If we observe distinct marginals $\{p(\cdot, t_i)\}_{i=1}^3$ from an SDE in \mathcal{S} , such that the measurement times $\{t_i\}_{i=1}^3$ are uniformly sampled, i.e. $t_i \sim \text{Unif}[T_i, T_{i+1}]$, for some $0 < T_1 < T_2 < T_3 < T_4$, then, with probability 1, this is the only SDE in \mathcal{S} with marginals $\{p(\cdot, t_i)\}_{i=1}^3$.

Proof. By the countability of \mathcal{S} , it suffices to prove that the event that any two distinct SDEs in \mathcal{S} share the same marginals at each of the times $\{t_i\}_{i=1}^3$, has probability 0. Denote their parameters by $(-\nabla\Psi_1, \sigma_1^2) \neq (-\nabla\Psi_2, \sigma_2^2)$ and their marginals by $(p(\cdot, t))_{t \geq 0}$ and $(q(\cdot, t))_{t \geq 0}$. Suppose for contradiction that if we sample $t_i \sim \text{Unif}[T_i, T_{i+1}]$, then we observe $p(\cdot, t_i) = q(\cdot, t_i) \forall i \in \{1, 2, 3\}$, with some nonzero probability.

Since we sample $t_i \sim \text{Unif}[T_i, T_{i+1}]$, then the set of coincidence times in each subinterval, $\mathcal{I}_i = \{t \in [T_i, T_{i+1}] \mid p(\cdot, t) = q(\cdot, t)\}$, must be infinite to ensure nonzero probability. By Bolzano-Weierstrass, we may construct the convergent sequence $t_1^{(n)} \rightarrow t_1^* \in [T_1, T_2]$, using times $t_1^{(n)} \in \mathcal{I}_1$, and the convergent sequence $t_2^{(n)} \rightarrow t_2^* \in [T_2, T_3]$, using times $t_2^{(n)} \in \mathcal{I}_2$. At the limit points, t_1^* and t_2^* , we have $p(\cdot, t_1^*) = q(\cdot, t_1^*)$ and $\frac{\partial}{\partial t} p(\cdot, t_1^*) = \frac{\partial}{\partial t} q(\cdot, t_1^*)$ (see Theorem A.2 and the proof of Hashimoto et al. [2016, Corollary 2]). Hence,

$$\mathcal{L}_{-\nabla\Psi_1, \sigma_1^2}^*(p(\cdot, t_1^*)) = \mathcal{L}_{-\nabla\Psi_2, \sigma_2^2}^*(p(\cdot, t_1^*)) \quad (11)$$

$$\mathcal{L}_{-\nabla\Psi_1, \sigma_1^2}^*(p(\cdot, t_2^*)) = \mathcal{L}_{-\nabla\Psi_2, \sigma_2^2}^*(p(\cdot, t_2^*)) \quad (12)$$

It then follows from Theorem 4.2 that (11) and (12) are both solved by at most one distribution μ . Thus, $\mu = p(\cdot, t_1^*) = p(\cdot, t_2^*)$. However, by Theorem A.3, the only marginal that can repeat at distinct times is the stationary Gibbs distribution p_{eq} . This follows from a variation of Boltzmann's H-theorem, which states that the marginals of a gradient-flow SDE (1) decrease free energy, which is uniquely minimized at p_{eq} [Jordan et al., 1998, Chafaï, 2015]. Both processes must therefore reach p_{eq} by t_1^* , such that $p(\cdot, t) = q(\cdot, t) = p_{\text{eq}}$ for all $t \geq t_1^*$. In particular, since t_1^* is in the first subinterval, we have $p(\cdot, t_2) = p(\cdot, t_3) = p_{\text{eq}}$, which contradicts the assumption that the marginals $\{p(\cdot, t_i)\}_{i=1}^3$ are distinct. \square

5 Tri-level SB-refinement: nn-APPEX

We have shown in Section 4 that the full SDE is identifiable from $N \geq 3$ distinct marginals, $(p(\cdot, t_i))_{i=1}^N$. Building on this, we propose Neural Network-based Alternating Projection Parameter Estimation from X_0 (nn-APPEX), an improved version of APPEX [Guan et al., 2024], which can learn the full SDE, beyond those with

linear drift. nn-APPEX searches for the true parameters $(-\nabla\Psi, \sigma^2)$ by alternating between trajectory inference, drift estimation, and diffusion estimation.

First, given a reference SDE Q , we solve a multi-marginal Schrödinger Bridge problem to infer a law on paths P . In particular, P minimizes $\text{KL}(P\|Q)$, while obeying the multi-marginal constraints, i.e. $P \in \Pi(p(\cdot, t_i)_{i=1}^N)$. Second, from these inferred trajectories, we perform a maximum likelihood estimation (MLE) of the drift $-\nabla\Psi$. For generality and tractability, we optimize over neural network parameters θ . Third, we use MLE to estimate the diffusion σ^2 . We then use the new drift and diffusion estimates to update the reference SDE Q for the next iteration. Formally, at iteration k , nn-APPEX performs the steps

$$P_k = \arg \min_{P \in \Pi(p(\cdot, t_i)_{i=1}^N)} \text{KL}(P\|Q_{-\nabla\Psi_{\theta_{k-1}}, \sigma_{k-1}^2}), \quad (13)$$

$$\theta_k = \arg \min_{\theta} \text{KL}(P_k\|Q_{-\nabla\Psi_{\theta}, \sigma_{k-1}^2}), \quad (14)$$

$$\sigma_k^2 = \arg \min_{\sigma^2} \text{KL}(P_k\|Q_{-\nabla\Psi_{\theta_k}, \sigma^2}), \quad (15)$$

and we iterate until convergence, or until a maximum number of iterations is reached. We emphasize that nn-APPEX does not require prior knowledge, since any gradient-flow SDE (1) can be used as the initial reference $Q_{-\nabla\Psi_{\theta_0}, \sigma_0^2}$. While it is known that the KL divergence on the space $C([0, T], \mathbb{R}^d)$ is infinite between SDEs with different diffusions [Shen et al., 2025], we note that given finite observation times, $\{t_i\}_{i=1}^N$, we may instead evaluate KL divergence on $C(\{t_i\}_{i=1}^N, \mathbb{R}^d)$, computed over the observed couplings $p_{t_i, t_{i+1}}$. As shown in Guan et al. [2024, Section 4] and Section D, this objective is finite for gradient-flow SDEs (1), and thus enables principled tri-level optimization.

The SB problem (13) is equivalent to entropic OT, and can thus be solved with iterative proportional fitting [Peyré et al., 2019]. For MLE parameter estimation on the inferred paths, we use the Euler-Maruyama approximation, and present derivations in Section E. In particular, the optimal drift parameters $\hat{\theta}$ are independent of σ^2 , since minimizing the negative log-likelihood with respect to θ is equivalent to minimizing

$$\ell(\theta) = \sum_{n=1}^N \sum_{k=0}^{T-1} \left\| x_{(k+1)\Delta t}^{(n)} - x_{k\Delta t}^{(n)} + \nabla\Psi_{\theta}(x_{k\Delta t}^{(n)}) \Delta t \right\|_2^2, \quad (16)$$

where N is the number of paths, T is the number of time steps, and Δt is the time step. We therefore estimate $-\nabla\Psi_{\hat{\theta}}$ by fitting a neural network whose parameters minimize $\ell(\theta)$, as done in Shen et al. [2025]. The diffusion MLE, $\hat{\sigma}^2$, is then derived from the quadratic

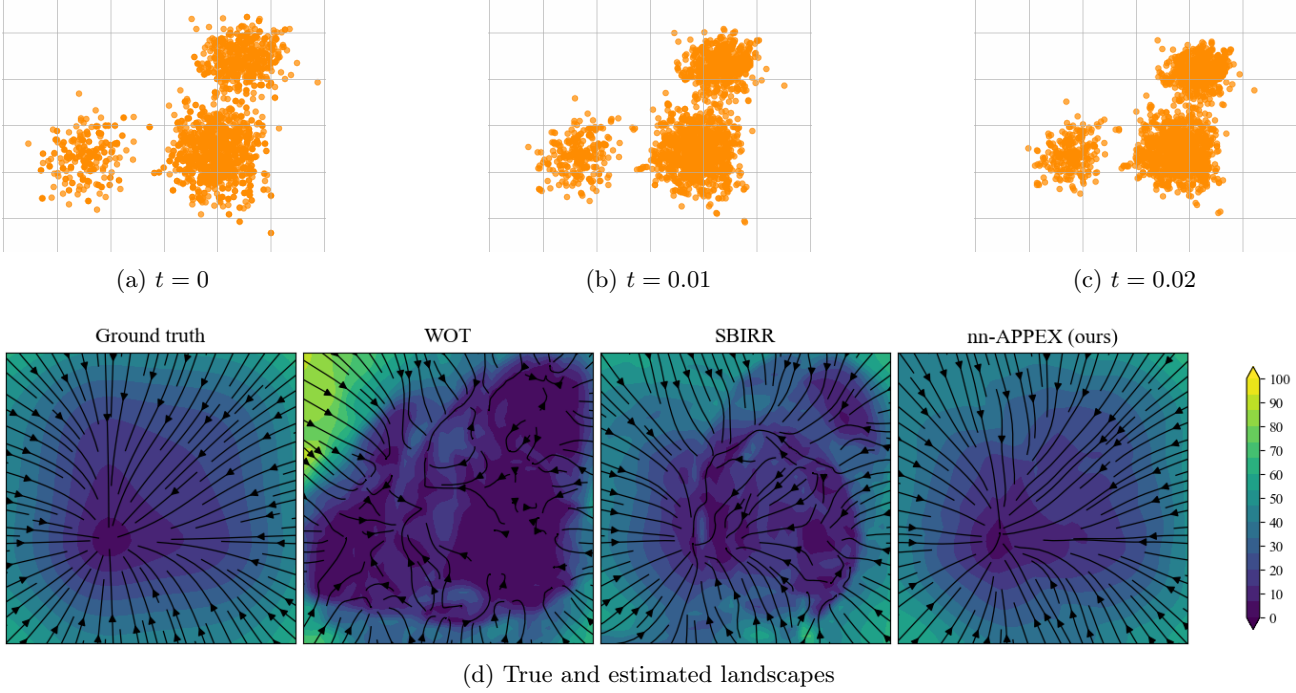


Figure 2: We simulate gradient-flow SDEs from a variety of potentials and provide inference methods with samples from three distinct marginals, initialized from a random Gaussian mixture model. Data for one seed is plotted for the Oakley–O’Hagan potential in (a)–(c), along with the true and estimated landscapes in (d).

variation, conditioned on the estimated drift $\nabla \Psi_{\hat{\theta}}$,

$$\hat{\sigma}^2 = \frac{1}{d N T \Delta t} \ell(\hat{\theta}). \quad (17)$$

By alternating between these three procedures, **nn-APPEX** iteratively reduces the divergence between *reconstructed paths*, $P \in \Pi(p(\cdot, t_i)_{i=1}^N)$, which obey the observed marginals, and *paths from the estimated gradient-flow SDE* with law Q :

$$\begin{aligned} \text{KL}(P_{k+1} \| Q_{-\nabla \Psi_{k+1}, \sigma_{k+1}^2}) &\leq \text{KL}(P_{k+1} \| Q_{-\nabla \Psi_{k+1}, \sigma_k^2}) \\ &\leq \text{KL}(P_{k+1} \| Q_{-\nabla \Psi_k, \sigma_k^2}) \leq \text{KL}(P_k \| Q_{-\nabla \Psi_k, \sigma_k^2}). \end{aligned} \quad (18)$$

We note that P need not be a gradient-flow SDE, and that Q need not respect the marginal constraints. In fact, by Theorem 4.3, only one gradient-flow SDE $Q_{-\nabla \Psi, \sigma^2}$ obeys the marginal constraints, which implies

$$\inf_{P \in \Pi(p(\cdot, t_i)_{i=1}^N)} \text{KL}(P \| Q_{-\nabla \Psi, \sigma^2}) = 0 \iff P = Q_{-\nabla \Psi, \sigma^2}.$$

By decreasing the relative divergence via (18), **nn-APPEX** iteratively approaches the unique true solution. However, convergence to the unique minimizer is an open question. We discuss our algorithm’s convergence and runtime in Section D.

To highlight distinctions with existing SB methods, we note differences in algorithmic design, relative to **nn-APPEX**:

- Waddington-OT (WOT) [Schiebinger et al., 2019] fixes the reference Q to be a Brownian motion with diffusivity σ^2 and stops after (14).
- SBIRR [Shen et al., 2025, Zhang, 2024] fixes σ^2 and iteratively performs steps (13) and (14).
- APPEX [Guan et al., 2024] iteratively performs all three steps, but uses closed form MLE solutions, specific to linear additive noise SDEs, for the drift and diffusion updates.

Each method reconstructs paths by solving a Schrödinger Bridge problem. However, these paths will be incorrect unless the reference SDE matches the true SDE. While **nn-APPEX** has the flexibility to re-estimate the gradient-flow drift as well as the diffusivity, previous methods cannot reliably determine a suitable reference SDE. WOT, and related methods [Lavenant et al., 2024, Forrow and Schiebinger, 2021, Chizat et al., 2022], fix a pure Brownian reference, which is incompatible with any nonzero potential. Although SBIRR adjusts its reference drift, if σ^2 is misspecified, then it would also misspecify the reference SDE, hindering its ability to learn the drift. While APPEX adjusts drift and diffusion, it estimates a misspecified SDE, unless the ground-truth potential Ψ happens to be quadratic.

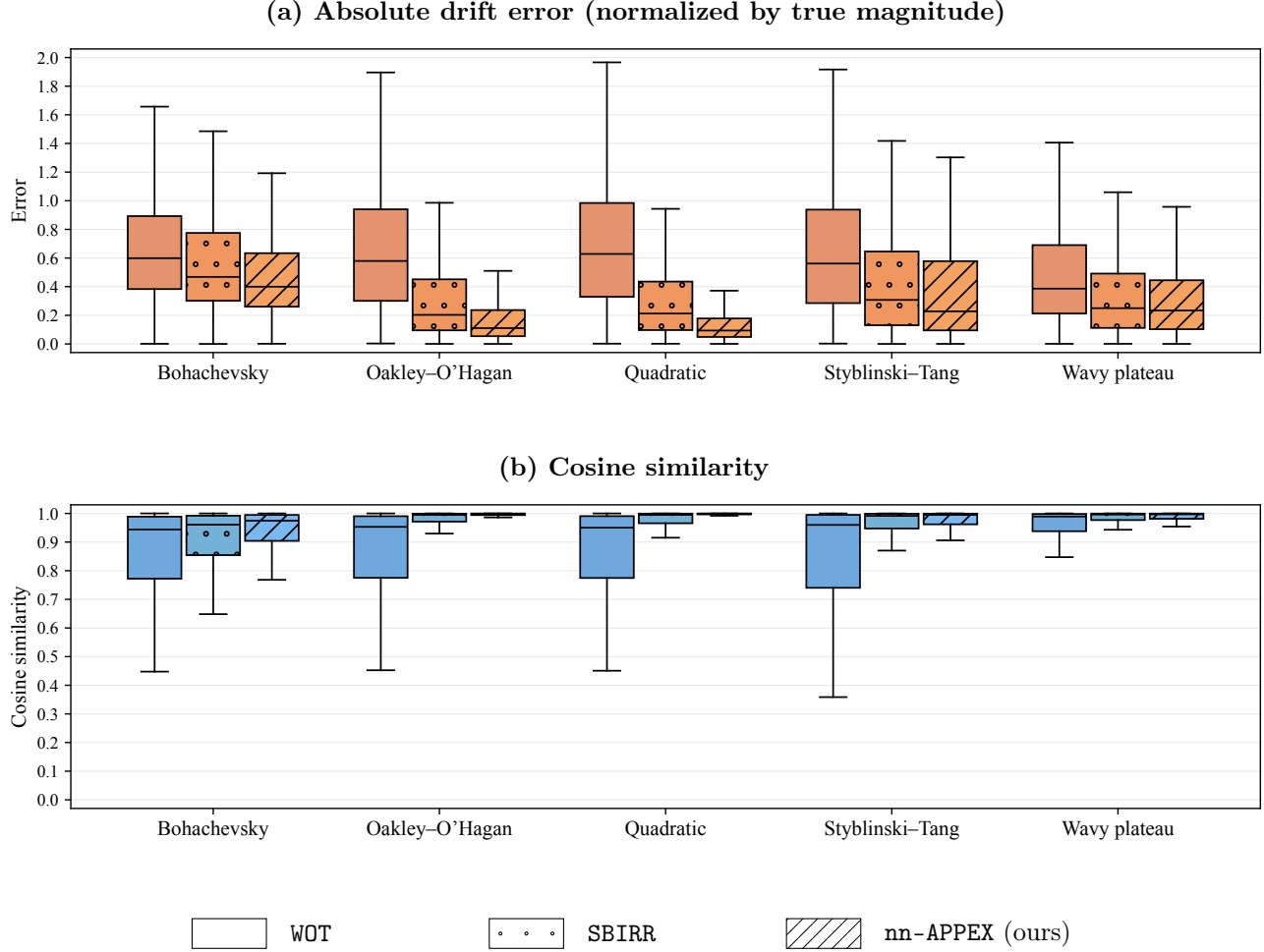


Figure 3: The ability of different Schrödinger Bridge methods to infer the gradient-flow drift is evaluated across five different potentials using (a) normalized absolute error (lower is better) and (b) cosine similarity (higher is better). Methods are given samples from three distinct marginals, such that the initial distribution is a Gaussian mixture model with randomly initialized components. The box-and-whisker plots aggregated from 10 seeds show that our method, **nn-APPEX**, performs the best across all potentials.

6 Experiments

In this section, we perform extensive experiments on simulated data to evaluate **nn-APPEX** against previous Schrödinger Bridge methods, **WOT** and **SBIRR**. The code repository is available on [GitHub](#).

6.1 Experimental setup

We explain details about the data, method implementation, and performance metrics below.

Data generation. To simulate gradient-flow SDEs, we fix the diffusivity $\sigma^2 = 0.2$ and consider five potentials that are commonly used as benchmarks in the literature [Terpin et al., 2024, Persiianov et al., 2025]. Potentials were chosen to ensure the existence of a stationary distribution $p_{\text{eq}} = \exp(-\frac{\Psi}{2\sigma^2})$. See Section F

for the list of potentials. For our main experiments, we initialize the first marginal as a random Gaussian mixture model (GMM), due to their universal approximation properties [McLachlan and Rathnayake, 2014] and their applicability for clustering scRNA data into different cell types [Yu et al., 2021]. We uniformly sample the number of components between 1 and 10, their means within $[-3, 3]^2$, and their variances between 0.5 and 1.0. We then mirror the “three marginals” identifiability setting from Theorem 4.3, by sampling $N = 2000$ points from the GMM initial distribution, then forward projecting these points using the Euler-Maruyama scheme for an additional 2 time steps of size $\Delta t = 0.01$. Experiments are repeated across 10 seeds for each SDE to ensure replicability. Marginals for one seed are pictured for the SDE driven by the Oakley-O'Hagan potential in Fig. 2(a)-(c).

Methods. To perform a systematic ablation that isolates the effects of iterative reference refinement and adaptive diffusion on inference, all methods are given the same data and initialization, and any shared sub-procedure is implemented identically across methods. To emulate the realistic scenario where the practitioner can only estimate the true diffusivity σ^2 up to an order of magnitude [Guan et al., 2024], we sample the diffusivity prior as $\sigma_{\text{prior}}^2 \sim \sigma^2 \times 10^{\text{Unif}[-1,1]}$, for each of the 10 seeds. This setting could be considered as favorable towards methods like WOT and SBIRR, since real-world diffusion estimates may in fact be off by two orders of magnitude [Forrow, 2024]. For all methods, the SB step (13) is solved using up to 200 iterations of a multi-marginal iterative proportional fitting procedure (IPFP) [Marino and Gerolin, 2020, Section 4.3], which rescales the per-time slice scalings until the marginal constraints are met up to an L^∞ error of 10^{-5} . 2000 trajectories are then sampled from the inferred law on paths. Similarly, each method performs the drift MLE step (14) by fitting a 3-layer multi-layer perceptron with `silu` activation, trained to minimize (16) via the Adam optimizer (epochs = 500 and learning_rate = 3×10^{-3}) [Kingma and Ba, 2014]. Only SBIRR and nn-APPEX are iterative, and we use 30 iterations for each method.

Metrics. We assess WOT, SBIRR, and nn-APPEX, by evaluating both the scale and shape of their resulting landscapes $\nabla\Psi_{\hat{\theta}}$ with respect to the true landscape $\nabla\Psi$. We use the following metrics, evaluated on 2601 points (51×51 point grid) within $[-4, 4]^2$:

- *Absolute error (normalized):* $\frac{|\nabla\Psi_{\hat{\theta}}(x) - \nabla\Psi(x)|}{\|\nabla\Psi(x)\|}$
- *Cosine similarity:* $\frac{\langle \nabla\Psi_{\hat{\theta}}(x), \nabla\Psi(x) \rangle}{\|\nabla\Psi_{\hat{\theta}}(x)\| \|\nabla\Psi(x)\|}$.

6.2 Results

The results are aggregated over 10 seeds for each gradient-flow SDE, and shown in Fig. 3. We see that nn-APPEX yields the best and most robust estimates for the drift landscapes. On each of the five SDEs, its estimates have the lowest absolute error, the highest cosine similarity, and the lowest variance. While SBIRR significantly outperforms WOT, due to iterative drift refinement, its inability to update its diffusion prior prevents it from learning the drift field to the same fidelity as nn-APPEX. In particular, WOT and SBIRR regularly orient flow lines incorrectly in low potential zones, due to misspecified diffusivity (see Fig. 2).

We also replicate this experiment such that instead of a GMM initialization, the initial distribution is either uniform, $p_0 \sim \text{Unif}[-4, 4]^2$, as done in previous work [Terpin et al., 2024], or given by the stationary Gibbs

distribution $p_0 \sim p_{\text{eq}}$. The results are summarized in Fig. 4 and Fig. 5 of the Supplement. For the uniform initialization, nn-APPEX continues to perform the best on all SDEs, and all methods perform relatively better, due to higher observability in the evaluation region $[-4, 4]^2$. For the Gibbs initialization, all methods fail at inference, which is consistent with identifiability theory (Theorem 4.1).

We also evaluate nn-APPEX against the state-of-the-art variational method JK0net* [Terpin et al., 2024] given GMM initializations. Results are plotted in Fig. 6 and show that nn-APPEX achieves more accurate drift and diffusion estimates.

7 Conclusions

This work provides a call to action for researchers in ML and single-cell biology to move beyond the current paradigm of assuming known diffusion for marginals-based SDE inference, as we show that this is not only unnecessary, but also problematic in practice. Our theoretical contributions resolve a longstanding identifiability problem by proving that the gradient-flow drift and the diffusivity are jointly identifiable if and only if we observe transient marginals. This is significant for practical applications, since transience is a common and testable condition. We further expand the practicality of our result by proving that only three distinct marginals are needed for identifiability. To translate this theory into practice, we introduced the first Schrodinger Bridge-based method, capable of inferring arbitrary gradient-flow drift and diffusivity. Extensive numerical experiments demonstrate that our method, nn-APPEX, outperforms previous SB methods, in the realistic scenario where diffusivity is unknown.

Limitations and future work. While our work contributes novel theory and methodology for SDE inference from marginals, we note several limitations, which point to important directions for future work. First, the gradient-flow SDE model (1) is prevalent in many fields, but it does not capture some important dynamics. In single-cell dynamics, one may expect rotational dynamics from non-conservative drift, due to genetic feedback loops. As another example, in hydrology, material heterogeneity requires modified models for drift and diffusion. Second, our theory was proven given exact observation of the marginals $p(\cdot, t)$. Rigorous asymptotic theory quantifying identifiability with finite-samples and observational noise would be useful to the community. Finally, there is still a gap in showing optimality of joint inference methods. While experiments show positive results, proving that nn-APPEX converges to the true parameters under basic conditions would mark a major advance.

Acknowledgments. We thank NSERC for their support for Vincent Guan and Joseph Janssen. Nicolas Lanzetti was supported by the NCCR Automation, a National Centre of Competence in Research, funded by the Swiss National Science Foundation (grant number 51NF40_225155). Elina Robeva was supported by a Canada CIFAR AI Chair and an NSERC Discovery Grant (DGECR-2020-00338). The authors would also like to thank United Therapeutics for supporting this research.

References

Jean-David Benamou, Guillaume Carlier, Simone Di Marino, and Luca Nenna. An entropy minimization approach to second-order variational mean-field games. *Mathematical Models and Methods in Applied Sciences*, 29(08):1553–1583, 2019.

Renato Berlinghieri, Yunyi Shen, Jialong Jiang, and Tamara Broderick. Oh snapmmd! forecasting stochastic dynamics beyond the schrödinger bridge's end. *arXiv preprint arXiv:2505.16082*, 2025.

Jaya PN Bishwal. *Parameter estimation in stochastic differential equations*. Springer, 2007.

Vladimir I Bogachev, Nicolai V Krylov, Michael Röckner, and Stanislav V Shaposhnikov. *Fokker–Planck–Kolmogorov Equations*, volume 207. American Mathematical Society, 2022.

Alexander P Browning, David J Warne, Kevin Burrage, Ruth E Baker, and Matthew J Simpson. Identifiability analysis for stochastic differential equation models in systems biology. *Journal of the Royal Society Interface*, 17(173):20200652, 2020.

Charlotte Bunne, Laetitia Papaxanthos, Andreas Krause, and Marco Cuturi. Proximal optimal transport modeling of population dynamics. In *International Conference on Artificial Intelligence and Statistics*, pages 6511–6528. PMLR, 2022.

Djalil Chafaï. From boltzmann to random matrices and beyond. In *Annales de la Faculté des sciences de Toulouse: Mathématiques*, volume 24, pages 641–689, 2015. no. 4.

Lénaïc Chizat, Stephen Zhang, Matthieu Heitz, and Geoffrey Schiebinger. Trajectory inference via mean-field Langevin in path space. *Advances in Neural Information Processing Systems*, 35:16731–16742, 2022.

Rick Durrett. *Probability: theory and examples*, volume 49. Cambridge university press, 2019.

Aden Forrow. Consistent diffusion matrix estimation from population time series. *arXiv preprint arXiv:2408.14408*, 2024.

Aden Forrow and Geoffrey Schiebinger. Lineageot is a unified framework for lineage tracing and trajectory inference. *Nature communications*, 12(1):4940, 2021.

Vincent Guan, Joseph Janssen, Hossein Rahmani, Andrew Warren, Stephen Zhang, Elina Robeva, and Geoffrey Schiebinger. Identifying drift, diffusion, and causal structure from temporal snapshots. *arXiv preprint arXiv:2410.22729*, 2024.

Wiebke Günther, Oana-Iuliana Popescu, Martin Rabel, Urmi Ninad, Andreas Gerhardus, and Jakob Runge. Causal discovery with endogenous context variables. *Advances in Neural Information Processing Systems*, 37:36243–36284, 2024.

Tatsunori Hashimoto, David Gifford, and Tommi Jaakkola. Learning population-level diffusions with generative rnns. In *International Conference on Machine Learning*, pages 2417–2426. PMLR, 2016.

Richard Jordan, David Kinderlehrer, and Felix Otto. The variational formulation of the fokker–planck equation. *SIAM journal on mathematical analysis*, 29(1):1–17, 1998.

Diederik P Kingma and Jimmy Ba. Adam: A method for stochastic optimization. *arXiv preprint arXiv:1412.6980*, 2014.

Hugo Lavenant, Stephen Zhang, Young-Heon Kim, and Geoffrey Schiebinger. Toward a mathematical theory of trajectory inference. *Ann. Appl. Probab.*, 34(1A), Feb 2024.

Tony Lelièvre and Gabriel Stoltz. Partial differential equations and stochastic methods in molecular dynamics. *Acta Numerica*, 25:681–880, 2016.

Fadji Zaouna Maina and Erica R Siirila-Woodburn. Watersheds dynamics following wildfires: Nonlinear feedbacks and implications on hydrologic responses. *Hydrological Processes*, 34(1):33–50, 2020.

Simone Di Marino and Augusto Gerolin. An optimal transport approach for the schrödinger bridge problem and convergence of sinkhorn algorithm. *Journal of Scientific Computing*, 85(2):27, 2020.

Geoffrey J McLachlan and Suren Rathnayake. On the number of components in a gaussian mixture model. *Wiley Interdisciplinary Reviews: Data Mining and Knowledge Discovery*, 4(5):341–355, 2014.

Stéphane Menozzi, Antonello Pesce, and Xicheng Zhang. Density and gradient estimates for non degenerate brownian sdes with unbounded measurable drift. *Journal of Differential Equations*, 272:330–369, 2021.

Nilah Monnier, Syuan-Ming Guo, Masashi Mori, Jun He, Péter Lénárt, and Mark Bathe. Bayesian approach to msd-based analysis of particle motion in live cells. *Biophysical journal*, 103(3):616–626, 2012.

Kirill Neklyudov, Rob Brekelmans, Daniel Severo, and Alireza Makhzani. Action matching: Learning stochastic dynamics from samples. In *International conference on machine learning*, pages 25858–25889. PMLR, 2023.

Jan Nygaard Nielsen, Henrik Madsen, and Peter C Young. Parameter estimation in stochastic differential equations: an overview. *Annual Reviews in Control*, 24:83–94, 2000.

Bernt Oksendal. *Stochastic differential equations: an introduction with applications*. Springer Science & Business Media, 2013.

Grigoris A Pavliotis. Stochastic processes and applications. *Texts in Applied Mathematics*, 60, 2014.

Asger Roer Pedersen. A new approach to maximum likelihood estimation for stochastic differential equations based on discrete observations. *Scandinavian journal of statistics*, pages 55–71, 1995.

Mikhail Persiianov, Jiawei Chen, Petr Mokrov, Alexander Tyurin, Evgeny Burnaev, and Alexander Krotin. Learning of population dynamics: Inverse optimization meets jko scheme. *arXiv preprint arXiv:2506.01502*, 2025.

Gabriel Peyré, Marco Cuturi, et al. Computational optimal transport: With applications to data science. *Foundations and Trends® in Machine Learning*, 11(5-6):355–607, 2019.

Hannes Risken. Fokker-planck equation. In *The Fokker-Planck equation: methods of solution and applications*, pages 63–95. Springer, 1989.

Jakob Runge, Sebastian Bathiany, Erik Boltt, Gustau Camps-Valls, Dim Coumou, Ethan Deyle, Clark Glymour, Marlene Kretschmer, Miguel D Mahecha, Jordi Muñoz-Marí, et al. Inferring causation from time series in earth system sciences. *Nature communications*, 10(1):2553, 2019.

Geoffrey Schiebinger, Jian Shu, Marcin Tabaka, Brian Cleary, Vidya Subramanian, Aryeh Solomon, Joshua Gould, Siyan Liu, Stacie Lin, Peter Berube, et al. Optimal-transport analysis of single-cell gene expression identifies developmental trajectories in reprogramming. *Cell*, 176(4):928–943, 2019.

Jan Seibert, Jeffrey J McDonnell, and Richard D Woodsmith. Effects of wildfire on catchment runoff response: a modelling approach to detect changes in snow-dominated forested catchments. *Hydrology research*, 41(5):378–390, 2010.

Yunyi Shen, Renato Berlinghieri, and Tamara Broderick. Multi-marginal schrödinger bridges with iterative reference refinement. In *International Conference on Artificial Intelligence and Statistics*, pages 3817–3825. PMLR, 2025.

Daniel W. Stroock. *Partial Differential Equations for Probabilists*. Cambridge Studies in Advanced Mathematics. Cambridge University Press, 2008.

Antonio Terpin, Nicolas Lanzetti, and Florian Dörfler. Learning diffusion at lightspeed. *arXiv preprint arXiv:2406.12616*, 2024.

Cole Trapnell, Davide Cacchiarelli, Jonna Grimsby, Prapti Pokharel, Shuqiang Li, Michael Morse, Niall J Lennon, Kenneth J Livak, Tarjei S Mikkelsen, and John L Rinn. The dynamics and regulators of cell fate decisions are revealed by pseudotemporal ordering of single cells. *Nature biotechnology*, 32(4):381–386, 2014.

Francisco Vargas, Pierre Thodoroff, Austen Lamacraft, and Neil Lawrence. Solving schrödinger bridges via maximum likelihood. *Entropy*, 23(9):1134, 2021.

Elias Ventre, Aden Forrow, Nitya Gadhiwala, Parijat Chakraborty, Omer Angel, and Geoffrey Schiebinger. Trajectory inference for a branching sde model of cell differentiation. *arXiv preprint arXiv:2307.07687*, 2023.

CH Waddington. How animal develop, 1935.

Yuanyuan Wang, Xi Geng, Wei Huang, Biwei Huang, and Mingming Gong. Generator identification for linear sdes with additive and multiplicative noise. *Advances in Neural Information Processing Systems*, 36, 2024.

Caleb Weinreb, Samuel Wolock, Betsabeh K Tusi, Merav Socolovsky, and Allon M Klein. Fundamental limits on dynamic inference from single-cell snapshots. *Proceedings of the National Academy of Sciences*, 115(10):E2467–E2476, 2018.

Grace Hui Ting Yeo, Sachit D Saksena, and David K Gifford. Generative modeling of single-cell time series with prescient enables prediction of cell trajectories with interventions. *Nature communications*, 12(1):3222, 2021.

Bin Yu, Chen Chen, Ren Qi, Ruiqing Zheng, Patrick J Skillman-Lawrence, Xiaolin Wang, Anjun Ma, and Haiming Gu. scgmai: a gaussian mixture model for clustering single-cell rna-seq data based on deep autoencoder. *Briefings in bioinformatics*, 22(4):bbaa316, 2021.

Stephen Zhang, Anton Afanassiev, Laura Greenstreet, Tetsuya Matsumoto, and Geoffrey Schiebinger. Optimal transport analysis reveals trajectories in steady-state systems. *PLoS computational biology*, 17(12):e1009466, 2021.

Stephen Y Zhang. Joint trajectory and network inference via reference fitting. In *Machine Learning in Computational Biology*, pages 72–85. PMLR, 2024.

A Theoretical background

A.1 The distributional definition of the Fokker-Planck equation

The Fokker-Planck equation defines the evolution of an SDE's marginals. For an overdamped Langevin SDE (1), its Fokker-Planck equation is given by

$$\frac{\partial p(x, t)}{\partial t} = \mathcal{L}_{-\nabla\Psi, \sigma^2}^*(p(\cdot, t))(x), \quad (19)$$

where the Fokker-Planck operator $\mathcal{L}_{-\nabla\Psi, \sigma^2}^*$ is defined as

$$(\mathcal{L}_{-\nabla\Psi, \sigma^2}^* p)(x) = \nabla \cdot (p(x) \nabla\Psi(x)) + \frac{\sigma^2}{2} \Delta p(x).$$

However, the equation (19) cannot be interpreted as a strong pointwise equality unless p is a twice differentiable probability density and $\Psi \in C^2(\mathbb{R}^d)$, which is a stronger condition than Lipschitz continuity of $\nabla\Psi$. To show that the evolution of marginals remains well-defined when we consider a general probability measure μ with finite second moments, we consider the weak distributional formulation of the Fokker-Planck equation (19) through its adjoint operator,

$$(\mathcal{L}_{-\nabla\Psi, \sigma^2} f)(x) = -\nabla\Psi(x) \cdot \nabla f(x) + \frac{\sigma^2}{2} \Delta f(x).$$

Consider now a family of Borel locally finite measures on $\mathbb{R}^d \times (0, T)$, which we denote by $(\mu_t)_{t \in (0, T)}$. To define weak solutions, we follow [Bogachev et al., 2022, Definition 6.1.1, Proposition 6.1.2(ii)] and say that $(\mu_t)_{t \in (0, T)}$ solves the Fokker-Planck equation for the initial condition $\mu|_{t=0} = \nu$ in the weak sense if for all test functions $\varphi \in C_0^\infty(\mathbb{R}^d)$, we have that

$$\int_{\mathbb{R}^d} \varphi(x) d\mu_t(x) - \int_{\mathbb{R}^d} \varphi(x) d\nu(x) = \lim_{\tau \rightarrow 0+} \int_\tau^t \int_{\mathbb{R}^d} \mathcal{L}_{-\nabla\Psi, \sigma^2} \varphi(x) d\mu_s(x) ds \quad (20)$$

for almost all $t \in [0, T]$. This can be denoted using the compact notation

$$\partial_t \mu = \mathcal{L}_{-\nabla\Psi, \sigma^2}^* \mu. \quad (21)$$

In this setting, the existence and uniqueness of a weak solution follows from [Bogachev et al., 2022, Theorem 9.4.8, Example 9.4.7], which applies because σ^2 is constant and we assumed that $\nabla\Psi$ is Lipschitz and obeys the growth condition, $\|\nabla\Psi(x)\| \leq K(1 + \|x\|)$. This result is also given in Stroock [2008, Theorem 1.1.9], which additionally shows that the family $(\mu_t)_{t \in (0, T)}$ is continuous, under the topology of weak convergence. Thus, the evolution of marginals can be identified with a continuous transition probability function, even under the weak formulation.

A.2 Additional proofs

The following results are used to complete the proof of Theorem 4.3. Since the observed marginals in Theorem 4.3 are sampled after some time $T_1 > 0$, we note that it suffices to consider times $t \geq T_1 > 0$. Also recall that for this result, we assume that $\Psi \in C^\infty(\mathbb{R}^d)$. This facilitates the proof, by ensuring that any marginal $p(\cdot, t)$ of a candidate gradient-flow SDE exhibits nice regularity and decay. Indeed, by elliptic regularity theory, the Fokker-Planck operator $\mathcal{L}_{-\nabla\Psi, \sigma^2}$ smooths marginals within any finite time.

Lemma A.1 (Finite-time smoothing of marginals). *Suppose that the potential of the gradient-flow SDE (1) is smooth, i.e. $\Psi \in C^\infty(\mathbb{R}^d)$. Then, for any positive time $t > 0$, it follows that the marginal $p(\cdot, t)$ admits a twice differentiable density, which obeys the Gaussian decay estimates*

$$\begin{aligned} p(x, t) &\leq K t^{-\frac{d+2}{2}} \exp\left(-\frac{\delta}{2t} \|x\|^2\right) \\ \|\nabla p(x, t)\| &\leq K t^{-\frac{d+2}{2}} \exp\left(-\frac{\delta}{2t} \|x\|^2\right) \end{aligned}$$

for some $K, \delta > 0$.

Proof. This result is given by Pavliotis [2014, Theorem 4.1]. However, we note that in the setup of this theorem, the initial distribution $p(\cdot, 0)$ is assumed to have a density. Thus, we first apply the density estimates from Menozzi et al. [2021, Theorem 1.2] to show that for any positive time $t/2 > 0$, the marginal $p(\cdot, t/2)$ admits a density, even if $p(\cdot, 0)$ is only a probability measure μ_0 . Indeed, by Menozzi et al. [2021, Theorem 1.2], the SDE admits a transition density function, $p(x, t|y, 0)$. Therefore, $p(\cdot, t) = \mu_0 * p(\cdot, t| \cdot, 0)$ admits a density, since it is the convolution of a probability measure with a probability density [Durrett, 2019, Theorem 2.1.16]. We may thus apply Pavliotis [2014, Theorem 4.1] after setting the initial density as the density of $p(\cdot, t/2)$. By combining these two PDE regularity theorems, we obtain the desired regularity and decay properties. \square

Lemma A.2 (Equivalence of marginals and of flows at accumulation point). *As defined in Theorem 4.3, let $\mathcal{I}_i = \{t \in [T_i, T_{i+1}] \mid p(\cdot, t) = q(\cdot, t)\}$, and let $\{t_n\}_{n \geq 0}$ be a sequence of times in \mathcal{I}_i , which converges to t_i^* . Then, $p(\cdot, t_i^*) = q(\cdot, t_i^*)$ and $\frac{\partial}{\partial t} p(\cdot, t_i^*) = \frac{\partial}{\partial t} q(\cdot, t_i^*)$.*

Proof. First, we define the map $f(t) : t \in [T_i, T_{i+1}] \rightarrow p(\cdot, t) - q(\cdot, t)$, where we recall that $T_i > 0$. Then, by Theorem A.1, for any $t \geq T_i$, $p(\cdot, t)$ and $q(\cdot, t)$ each admit a smooth density. Since we also have $\Psi \in C^\infty(\mathbb{R}^d)$, it follows that the Fokker-Planck equation (4) is defined pointwise, which implies the existence of the time derivatives $\frac{\partial p(x, t)}{\partial t}$ and $\frac{\partial q(x, t)}{\partial t}$ [Pavliotis, 2014, Theorem 4.1]. Thus, $f(t) = p(\cdot, t) - q(\cdot, t)$ is also a strongly differentiable map in $[T_i, T_{i+1}]$. From this, we deduce that \mathcal{I}_i is closed, since $\mathcal{I}_i = f^{-1}(\{0\})$, which is the preimage of a closed set under a continuous map. Since t_i^* is the limit point of a sequence $\{t_n\}_{n \in \mathbb{N}}$ in \mathcal{I}_i , it follows that t_i^* is also in the coincidence set \mathcal{I}_i , which proves that $p(\cdot, t_i^*) = q(\cdot, t_i^*)$. In fact, since they each admit densities, this is equivalent to the pointwise equality, $p(x, t_i^*) = q(x, t_i^*) \forall x \in \mathbb{R}^d$. Then, to prove that $\frac{\partial}{\partial t} p(\cdot, t_i^*) = \frac{\partial}{\partial t} q(\cdot, t_i^*)$, we recall that $p(\cdot, t)$ and $q(\cdot, t)$ are strongly differentiable in time, such that, for all $x \in \mathbb{R}^d$,

$$\begin{aligned} \frac{\partial}{\partial t} p(x, t_i^*) &= \lim_{t_n \rightarrow t_i^*} \frac{p(x, t_n) - p(x, t_i^*)}{t_n - t_i^*} \\ \frac{\partial}{\partial t} q(x, t_i^*) &= \lim_{t_n \rightarrow t_i^*} \frac{q(x, t_n) - q(x, t_i^*)}{t_n - t_i^*}. \end{aligned}$$

Then, by convergence of the sequence $t_n \rightarrow t_i^*$, the fact that $p(x, t_n) = q(x, t_n)$ (by construction of the sequence) and $p(x, t_i^*) = q(x, t_i^*)$, it follows that $\frac{\partial}{\partial t} p(x, t_i^*) = \frac{\partial}{\partial t} q(x, t_i^*)$ for all $x \in \mathbb{R}^d$. \square

Proposition A.3 (H-Theorem: marginals of gradient-flow SDEs monotonically decrease free energy). *Let $(p(\cdot, t))_{t \geq T_1}$ be the marginals of a Langevin SDE (1) from the earliest possible observation time in the setting of Theorem 4.3, and suppose that $\Psi \in C^\infty(\mathbb{R}^d)$. Then, the free energy $J(\rho) = \int_{\mathbb{R}^d} \Psi(x) \rho(x) dx + \beta \int_{\mathbb{R}^d} \rho(x) \log \rho(x) dx$, such that $\beta = \frac{\sigma^2}{2}$, strictly decreases in time, unless the process is at its stationary Gibbs distribution, p_{eq} . Thus, p_{eq} is the only possible marginal that can repeat at distinct times.*

Proof. We apply Theorem A.1, which implies that for all $t \geq T_1$, $p(\cdot, t)$ admits a twice differentiable density, with the exponential decay on both the density $p(x, t) \leq Kt^{\frac{-d+2}{2}} \exp(-\frac{\delta}{2t} \|x\|^2)$ and the gradient $\|\nabla p(x, t)\| \leq Kt^{\frac{-d+2}{2}} \exp(-\frac{\delta}{2t} \|x\|^2)$, for some $K, \delta > 0$. Thus, we may use chain rule, substitute the Fokker-Planck equation, and integrate by parts (with all boundary terms vanishing) to obtain

$$\frac{d}{dt} J(p(\cdot, t)) = \int_{\mathbb{R}^d} (\Psi(x) + \beta(\log p(x, t) + 1)) \frac{\partial}{\partial t} p(x, t) dx \quad (22)$$

$$= \int_{\mathbb{R}^d} (\Psi(x) + \beta(\log p(x, t) + 1)) [\nabla \cdot (p(x, t) \nabla \Psi(x)) + \beta \Delta p(x, t)] dx \quad (23)$$

$$= - \int_{\mathbb{R}^d} |\nabla \Psi(x)|^2 p(x, t) dx - 2\beta \int \nabla p(x, t) \cdot \nabla \Psi(x) dx - \beta^2 \int \frac{|\nabla p(x, t)|^2}{p(x, t)} dx \quad (24)$$

$$= - \int_{\mathbb{R}^d} p(x, t) \|\nabla \Psi(x) + \beta \nabla \log p(x, t)\|^2 dx \leq 0, \quad (25)$$

which has equality only if $\log p(x, t) + \frac{\Psi(x)}{\beta} = K$ for some constant K . It follows that the Gibbs distribution

$$p_{\text{eq}}(x) = \frac{1}{Z_{\Psi, \sigma^2}} \exp\left(-\frac{2\Psi(x)}{\sigma^2}\right),$$

is the only possible marginal, observed from $t \geq T_1$, which induces no change in free energy $J(p(\cdot, t))$. Moreover, by Theorem A.4, we note that $J(p(\cdot, t)) < \infty$. Each transient marginal in the evolution $(p(\cdot, t))_{t \geq T_1}$ therefore has a distinct well-defined free energy, which strictly decreases in time, unless we are at $p_{\text{eq}}(x)$. We conclude that the only possible re-occurring marginal in the observation period $t \geq T_1$ is the Gibbs distribution p_{eq} , which is the unique stationary distribution as long as it is integrable [Bogachev et al., 2022][Theorem 4.1.11]. \square

Lemma A.4 (Finite free energy). *Let $p(\cdot, t)$ satisfy $p(x, t) \leq Kt^{\frac{-d+2}{2}} \exp(-\frac{\delta}{2t}\|x\|^2)$ for some $K, \delta > 0$. Then, $J(p(\cdot, t)) = \int_{\mathbb{R}^d} \Psi(x)p(x, t)dx + \beta \int_{\mathbb{R}^d} p(x, t) \log(p(x, t))dx < \infty$, with $\beta = \frac{\delta^2}{2}$.*

Proof. By the fundamental theorem of calculus along the segment $t \mapsto tx$,

$$\Psi(x) - \Psi(0) = \int_0^1 \nabla \Psi(tx) \cdot x \, dt.$$

Then, since we have the linear growth condition, $\|\nabla \Psi(x)\| \leq K(1 + \|x\|)$ for all $x \in \mathbb{R}^d$, we have

$$|\Psi(x)| \leq |\Psi(0)| + \|x\| \int_0^1 \|\nabla \Psi(tx)\| \, dt \leq |\Psi(0)| + \|x\| \int_0^1 K(1 + t\|x\|) \, dt = |\Psi(0)| + K\|x\| + \frac{K}{2}\|x\|^2.$$

This bound shows that if $p(\cdot, t)$ has finite second moments, then the potential energy term $\int_{\mathbb{R}^d} \Psi(x)p(x, t)dx$ in the free energy is bounded. Since we always assume that the initial distribution has finite second moments, then $p(\cdot, t)$ also has finite second moments (see [Stroock, 2008, Theorem 1.1.9]).

We now control the second term in the free energy, by showing that $p(\cdot, t)$ has finite differential entropy. It suffices to apply the Gaussian decay estimate $p(x, t) \leq Kt^{\frac{-d+2}{2}} \exp(-\frac{\delta}{2t}\|x\|^2)$. By direct computation,

$$\begin{aligned} \int_{\mathbb{R}^d} p(x, t) \log p(x, t) \, dx &\leq \int_{\mathbb{R}^d} p(x, t) [\log K + \frac{-d+2}{2} \log t - \frac{\delta}{2t}\|x\|^2] \, dx \\ &\leq \log K \int p(x, t) \, dx + \frac{-d+2}{2} \log t \int p(x, t) \, dx - \frac{\delta}{2t} \int \|x\|^2 p(x, t) \, dx \\ &= \log K + \frac{-d+2}{2} \log t - \frac{\delta}{2t} \mathbb{E}_{p(\cdot, t)}[\|x\|^2] < \infty, \end{aligned}$$

since $p(\cdot, t)$ is a probability density with finite second moments. We therefore conclude that the free energy

$$J(p(\cdot, t)) = \int_{\mathbb{R}^d} \Psi(x)p(x, t) \, dx + \beta \int_{\mathbb{R}^d} p(x, t) \log p(x, t) \, dx < \infty$$

\square

We emphasize that Theorem A.3 is a classical result, which is well known in the stochastic analysis and statistical mechanics literature, where it is commonly referred to as an H-theorem, due to its connection to Boltzmann's second law of thermodynamics [Chafaï, 2015]. For example, [Jordan et al., 1998] states that given that $\Psi \in C^\infty(\mathbb{R}^d)$ and $p(\cdot, 0)$ is a density with finite free energy, then it is known in the literature (e.g. [Risken, 1989] and attached references) that $J(\rho)$ is a monotone functional on the marginals of a gradient-flow SDE (1), and that $J(\rho)$ is uniquely minimized at the stationary Gibbs distribution. While we have derived a proof of this result, we believe that the statement holds under more relaxed conditions. In particular, we use the assumption $\Psi \in C^\infty(\mathbb{R}^d)$ to derive the regularity and decay estimates from Theorem A.1, which we frequently use for our proof. However, we believe that existing results in parabolic elliptic PDE theory should yield the same estimates under milder assumptions. We note that a proof is given in [Chafaï, 2015, Sec. 1.7], provided that the Gibbs distribution is integrable, and [Jordan et al., 1998] notes that the monotonicity holds, even if the Gibbs distribution is not integrable, but it is unclear what conditions are required.

B Identifiability in the time-inhomogeneous case

Theorem 4.2 assumes that the drift and diffusion terms are time-homogeneous. However, many physical systems have time-inhomogeneous dynamics. For example, in hydrology, extreme events, such as droughts or fires, can

cause “regime shifts” in the underlying functional relationships [Runge et al., 2019, Günther et al., 2024, Pedersen, 1995, Seibert et al., 2010, Maina and Siirila-Woodburn, 2020]. We may define this notion for gradient-flow SDEs, such that the drift and diffusion terms change due to regime shifts at specific times $\{t_i\}_{i=0}^{n-1}$ (with the drift remaining smooth and satisfying the growth condition in each regime to ensure well-posedness).

Definition B.1 (Time-inhomogeneous gradient-flow SDE with discrete regimes). *A time-inhomogeneous Langevin SDE with discrete regimes, marked by events taking place at times $\{t_i\}_{i=0}^{n-1}$, is given by*

$$dX_t = -\nabla\Psi(X_t, t_i)dt + \sigma(t_i)dW_t, \quad (26)$$

such that $\nabla\Psi(X_t, t)$ and $\sigma(t)^2$ are time-homogeneous within each regime $t \in [t_i, t_{i+1})$.

Under these time-inhomogeneous dynamics, identifiability, which is defined analogously to the time-homogeneous case, is still guaranteed by transient marginals.

Corollary B.2 (Identifiability for time-inhomogeneous gradient-flow SDEs with discrete regimes). *The time-inhomogeneous gradient-flow SDE with discrete regimes (26) is identifiable from its marginals $(p(\cdot, t))_{t \in [0, T]}$ if and only if $p(\cdot, t_i)$ is not a stationary distribution of $dX_t = \nabla\Psi(X_t, t_i)dt + \sigma(t_i)dW_t$ for each t_i .*

Proof. We apply Theorem 4.2 on each regime $[t_i, t_{i+1})$. Since the regimes form a partition of $[0, T]$, this guarantees that there is a unique SDE with the observed marginals $(p(\cdot, t))_{t \in [0, T]}$. \square

Intuitively, the drift and diffusion within a given regime $[t_i, t_{i+1})$ are identifiable if and only if the regime’s initial marginal, $p(\cdot, t_i)$, is not a stationary distribution. However, we note that if the drift or diffusion terms change continuously in time, then it no longer follows that transience completely characterizes identifiability. Indeed, the process could be in an equilibrium state that itself is changing in time, as the next example shows. In particular, distinct time-inhomogeneous SDEs may share the same marginals $(p(\cdot, t))_{t \geq 0}$, as long as for each $t \geq 0$, the marginal $p(\cdot, t)$ is precisely the stationary distribution of the time-inhomogeneous residual process, evaluated at that time.

Example B.3 (Continuously evolving equilibrium due to time-inhomogeneous potential). *The SDEs*

$$dX_t = dW_t, \quad (27)$$

$$dY_t = \begin{cases} dW_t, & t = 0, \\ -\frac{Y_t}{t} dt + \sqrt{3} dW_t, & t > 0. \end{cases} \quad (28)$$

produce the same marginals $p(\cdot, t) = \mathcal{N}(0, t)$ when initialized with $X_0 = Y_0 = 0$, i.e., $p_0 = \delta(x)$.

Proof. Let $t > 0$. The respective Fokker-Planck operators for both SDEs are

$$\begin{aligned} \mathcal{L}_{0,1}^*(p(\cdot, t))(x) &= \frac{1}{2} \frac{\partial^2}{\partial x^2} p(x, t) \\ \mathcal{L}_{-\frac{x}{t}, 3}^*(p(\cdot, t))(x) &= \frac{\partial}{\partial x} \left(p(x, t) \frac{x}{t} \right) + \frac{3}{2} \frac{\partial^2}{\partial x^2} p(x, t) \end{aligned}$$

Then, suppose that $p(\cdot, t) = \mathcal{N}(0, t)$, such that $p(x, t) = \frac{1}{\sqrt{2\pi t}} \exp\left(-\frac{x^2}{2t}\right)$. Then,

$$\begin{aligned} \frac{\partial}{\partial x} p(x, t) &= -\frac{x}{t} p(x, t) \\ \frac{\partial^2}{\partial x^2} p(x, t) &= -\frac{p(x, t)}{t} + \frac{x^2}{t^2} p(x, t) \end{aligned}$$

It follows that

$$\begin{aligned}
 \mathcal{L}_{0,1}^*(p(\cdot, t))(x) &= -\frac{p(x, t)}{2t} + \frac{x^2}{2t^2}p(x, t) \\
 &= \frac{p(x, t)}{2t^2}(x^2 - t) \\
 \mathcal{L}_{-\frac{x}{t}, 3}^*(p(\cdot, t))(x) &= -\frac{x^2}{t^2}p(x, t) + \frac{p(x, t)}{t} + \frac{3x^2}{2t^2}p(x, t) - \frac{3p(x, t)}{2t} \\
 &= \frac{p(x, t)}{2t^2}(-2x^2 + 2t + 3x^2 - 3t) \\
 &= \frac{p(x, t)}{2t^2}(x^2 - t).
 \end{aligned}$$

Thus, the Fokker-Planck operators are equivalent for $p(\cdot, t) = \mathcal{N}(0, t)$, which are the marginals of Brownian motion. Equivalently, we observe that $\mathcal{N}(0, t)$ is the stationary distribution of the residual Fokker-Planck equation at time t :

$$0 = \mathcal{L}_{-\frac{x}{t}, 2}^*(p_{\text{eq}})(x) = \frac{\partial}{\partial x} \left(p_{\text{eq}}(x) \frac{x}{t} \right) + \frac{\partial^2}{\partial x^2} p_{\text{eq}}(x).$$

Given $t > 0$, $p_{\text{eq}}(x) = \frac{1}{\sqrt{2\pi t}} \exp\left(-\frac{x^2}{2t}\right)$ solves the above equation. This yields the interpretation that the marginals are at equilibrium (for the residual process $dZ_t = -\frac{Z_t}{t}dt + \sqrt{2}dW_t$), which itself is time-varying. \square

C Additional non-identifiability examples

For gradient-flow SDEs, we have proven that non-identifiability from marginals arises if and only the observed marginals also correspond to the marginals of a residual process in equilibrium. An example for the time-homogeneous case was given in Theorem 3.2, such that the equilibrium marginals are constant, and an example for the time-inhomogeneous case was given in Theorem B.3, such that the equilibrium distribution of the residual process continuously changes in time.

However, for other forms of SDEs, other types of non-identifiability have been documented in the literature, including: undetectable rotations [Weinreb et al., 2018, Shen et al., 2025, Guan et al., 2024], rank-degenerate trajectories [Wang et al., 2024], and sharing the same stationary distribution [Lavenant et al., 2024]. We overview examples below:

Example C.1 (Gaussian pancake [Guan et al., 2024]). Let $a, b, c \in \mathbb{R}$, with $a \leq b$, and let X_0 be defined as a 2d Gaussian pancake, such that for each fixed $x_0^{(2)} \in [a, b]$, the first coordinate $x_0^{(1)} \sim \mathcal{N}(0, 1)$:

$$dX_t = \begin{bmatrix} -1 & 0 \\ 0 & b \end{bmatrix} dt + \begin{bmatrix} 1 & 0 \\ 0 & c \end{bmatrix} dW_t, \quad X_0 \sim \mathcal{N}(0, 1) \times [a, b] \quad (29)$$

$$dY_t = \begin{bmatrix} -10 & 0 \\ 0 & b \end{bmatrix} dt + \begin{bmatrix} \sqrt{10} & 0 \\ 0 & c \end{bmatrix} dW_t, \quad Y_0 \sim \mathcal{N}(0, 1) \times [a, b] \quad (30)$$

Example C.2 (Rotation [Shen et al., 2025, Hashimoto et al., 2016, Weinreb et al., 2018, Guan et al., 2024]).

$$\begin{aligned}
 dX_t &= dW_t, & X_0 &\sim \mathcal{N}(0, I) \\
 dY_t &= \begin{bmatrix} 0 & 1 \\ -1 & 0 \end{bmatrix} Y_t dt + dW_t, & Y_0 &\sim \mathcal{N}(0, I)
 \end{aligned}$$

Example C.3 (Degenerate rank [Wang et al., 2024, Guan et al., 2024]).

$$\begin{aligned}
 dX_t &= \begin{bmatrix} 1 & 2 \\ 1 & 0 \end{bmatrix} X_t dt + \begin{bmatrix} 1 & 2 \\ -1 & -2 \end{bmatrix} dW_t, & X_0 &= \begin{bmatrix} 1 \\ -1 \end{bmatrix} \\
 dY_t &= \begin{bmatrix} 1/3 & 4/3 \\ 2/3 & -1/3 \end{bmatrix} Y_t dt + \begin{bmatrix} 1 & 2 \\ -1 & -2 \end{bmatrix} dW_t, & Y_0 &= \begin{bmatrix} 1 \\ -1 \end{bmatrix}
 \end{aligned}$$

D Convergence and runtime of nn-APPEX

To discuss convergence of nn-APPEX’s tri-level iterative scheme (13)-(15), we first rigorously justify why we may re-estimate diffusion while ensuring that the objective remains finite. In particular, we must show that we have finite KL divergence between the reconstructed paths from the step (13) and the paths following MLE parameter estimation of a gradient-flow SDE from the steps (14) and (15).

Given continuously observed marginals of a d -dimensional process, recall that the KL divergence between two laws on paths P and Q , taken over the path space $\Omega = C([0, T], \mathbb{R}^d)$, is given by

$$\text{KL}(Q \| P) = \int_{\Omega} \log \left(\frac{dQ}{dP}(\omega) \right) dQ(\omega). \quad (31)$$

By Girsanov’s theorem, (31) is only finite for Q and P , if their underlying SDEs share the same diffusion [Vargas et al., 2021]. Besides non-identifiability, this is another cited reason for why previous Schrodinger Bridge methods assume that diffusivity must be fixed [Shen et al., 2025]. However, in the practical setting, we only observe a finite number of marginals, so we should instead optimize KL divergence over the discretized path space $\Omega_N = C(\{t_i\}_{i=1}^N, \mathbb{R}^d)$. Then, for each law on paths, we only observe the couplings, $Q_{t_i, t_{i+1}}$ and $P_{t_i, t_{i+1}}$, between consecutive times. Let Q^N and P^N denote the concatenations of these couplings from t_1 to t_N . Then, by Benamou et al. [2019][Lemma 3.4], evaluating the KL divergence over $\Omega_N = C(\{t_i\}_{i=1}^N, \mathbb{R}^d)$ yields

$$\text{KL}(P^N \| Q^N) = \sum_{i=0}^{N-2} \text{KL}(P_{t_i, t_{i+1}} \| Q_{t_i, t_{i+1}}) - \sum_{i=1}^{N-2} \text{KL}(P_{t_i} \| Q_{t_i}). \quad (32)$$

First note that by the data processing inequality, $\text{KL}(P_{t_i} \| Q_{t_i}) \leq \text{KL}(P_{t_i, t_{i+1}} \| Q_{t_i, t_{i+1}})$. Hence, the expression will be finite as long as $\text{KL}(P_{t_i, t_{i+1}} \| Q_{t_i, t_{i+1}}) = \int_{\mathbb{R}^d \times \mathbb{R}^d} \log \left(\frac{dP_{t_i, t_{i+1}}}{dQ_{t_i, t_{i+1}}} \right) P_{t_i, t_{i+1}}(x) dx < \infty$. Since the transition density of any nondegenerate diffusion process is absolutely continuous with respect to the Lebesgue measure for any positive time, it follows that the expression is finite for all gradient-flow SDEs (1).

As noted in Section 5, the iterates will produce a monotonically decreasing sequence of KL divergences between reconstructed laws and MLE estimated laws. With the above argument, we have that the KL divergences are bounded above by some $M > 0$, and from below by 0 (attained by the true gradient-flow SDE parameters $(-\nabla \Psi, \sigma^2)$). Thus, the sequence of KL divergences must converge. However, as noted in Shen et al. [2025], this does not imply that the arguments necessarily converge, since multiple pairs (P, Q) may produce the same divergence, such that the iterative algorithm gets stuck in a cycle. While this has not been observed empirically, and is impossible if the divergence is 0 (since there is a unique gradient-flow SDE satisfying the marginal constraints), it is an open question whether the iterative scheme will converge to the unique optimal parameters. Indeed, while convergence of the iterative SB refinement algorithm has been proven in the case where the family of admissible probability transition densities is convex [Shen et al., 2025][Proposition 1], this condition does not generally hold, and is false for the family of gradient-flow SDEs.

D.1 Runtime

The runtime of nn-APPEX is split across its three subprocedures:

1. **Trajectory inference** (13): solving the multi-marginal SB problem with respect to the current reference SDE to infer and sample from a law on paths.
2. **MLE drift estimation** (14): training a neural network whose parameters minimize the objective (16) over the inferred paths.
3. **MLE diffusion estimation** (15): computing the quadratic variation (17) over the inferred paths, conditioned on the drift estimate.

We note that nn-APPEX’s runtime will vary for different implementations of these subprocedures. In particular, there are multiple approaches for solving the multi-marginal SB problem. One approach is to consider all contiguous pairs of marginals, and then to apply iterative proportional fitting (Sinkhorn’s algorithm) on each pair

to determine the distribution over couplings [Shen et al., 2025, Guan et al., 2024]. To enforce consistency across transitions, we instead apply a multi-marginal iterative proportional fitting across all marginals, see [Marino and Gerolin, 2020][(4.9)]. This algorithm is analogous to the two-marginals setting, but it instead rescales per-time slices for each marginal, rather than just the endpoints. We observed better accuracy for this approach, given the same stopping criteria and maximum number of iterations, and were thus able to reduce runtime with relatively fewer iterations. We similarly note that MLE drift estimation can be implemented using different neural network architectures and hyperparameters. The details of our optimization are provided in Section 6. In contrast, the diffusion MLE estimate is a closed formula, and is thus cheap to compute. We report the average runtime (in seconds) of each of the three subprocedures for a single iteration, run on our main experiments:

	Trajectory inference	Drift MLE	Diffusion MLE	Total
Average	3.842 ± 0.046	6.176 ± 0.061	0.011 ± 0.002	10.030 ± 0.065

Table 1: Average runtime per iteration (seconds) for each subprocedure, aggregated across all potentials.

Since we used 30 iterations of **nn-APPEX**, each SDE inference for our main experiments was approximately 5 minutes. Since the diffusion MLE is computationally negligible, **nn-APPEX** has virtually the same runtime as an analogous **SBIRR** algorithm. In contrast, **WOT** only comprises a single iteration, and thus has the fastest runtime.

Stopping criteria, such as thresholds on the drift and diffusion estimates of the iterates, or approximations of the KL objective based on the W^1, W^2 metrics or maximum mean discrepancy (MMD), can be enforced for better performance and faster runtime. However, we note that these evaluations tend to be computationally intensive themselves, since they either require evaluations on a discretized grid or an approximation of relative entropy.

E Maximum likelihood estimation for drift and diffusion

Let the parameters of a gradient-flow SDE (1) be given by drift $-\nabla\Psi_\theta(x)$ and diffusivity σ^2 . Then, if we apply the first-order Euler-Maruyama linear approximation, we have that $X_{t+\Delta t}|X_t \sim \mathcal{N}(X_t - \nabla\Psi_\theta(X_t)\Delta t, \sigma^2\Delta t)$. Hence, for a single observation of a trajectory $x_t \rightarrow x_{t+\Delta t}$,

$$p(x_{t+\Delta t}|x_t) = \frac{1}{(2\pi\sigma^2\Delta t)^{d/2}} \exp\left(-\frac{\|x_{t+\Delta t} - x_t + \nabla\Psi_\theta(x_t)\Delta t\|^2}{2\sigma^2\Delta t}\right).$$

The full negative log-likelihood function is therefore given by

$$l(\theta, \sigma^2|x_t, x_{t+\Delta t}) = -\log(p(x_{t+\Delta t}|x_t)) = \frac{d}{2}\log(2\pi\Delta t) + \frac{d}{2}\log(\sigma^2) + \frac{\|x_{t+\Delta t} - x_t + \nabla\Psi_\theta(x_t)\Delta t\|^2}{2\sigma^2\Delta t}. \quad (33)$$

The MLE parameters $(\hat{\theta}, \hat{\sigma}^2)$ minimize $l(\theta, \sigma^2|x_t, x_{t+\Delta t})$. However, note that θ only appears in the numerator of the last term. It follows that $\hat{\theta}$ minimizes the squared error of the finite difference, which we denote

$$\ell(\theta) = \|x_{t+\Delta t} - x_t + \nabla\Psi_\theta(x_t)\Delta t\|^2. \quad (34)$$

If we observe N independent trajectories over T time steps ($T+1$ observed times), let $X = \{x_{k\Delta t}^{(n)}, x_{(k+1)\Delta t}^{(n)} : n \in \{1, \dots, N\}, k \in \{0, \dots, T-1\}\}$. We similarly observe that the negative log-likelihood function is given by

$$l(\theta, \sigma^2|X) = -\log\left(\prod_{n=1}^N \prod_{k=0}^{T-1} p(x_{(k+1)\Delta t}^{(n)}|x_{k\Delta t}^{(n)})\right) = -\sum_{n=1}^N \sum_{k=0}^{T-1} \log(p(x_{(k+1)\Delta t}^{(n)}|x_{k\Delta t}^{(n)})),$$

and it follows that $\hat{\theta}$ would minimize the mean squared error

$$\ell(\theta) = \sum_{n=1}^N \sum_{k=0}^{T-1} \left\| x_{(k+1)\Delta t}^{(n)} - x_{k\Delta t}^{(n)} + \nabla\Psi_\theta(x_{k\Delta t}^{(n)})\Delta t \right\|_2^2. \quad (35)$$

To derive the diffusion MLE estimator, $\hat{\sigma}^2$, we first fix $\theta = \hat{\theta}$, since the drift parameter can be independently optimized. Then, we solve $\frac{\partial}{\partial \sigma^2} l(\hat{\theta}, \sigma^2 | X) = 0$, and obtain

$$\begin{aligned} 0 &= \sum_{n=1}^N \sum_{k=0}^{T-1} \frac{d}{2\sigma^2} - \frac{1}{2\sigma^4 \Delta t} \sum_{n=1}^N \sum_{k=0}^{T-1} \left\| x_{(k+1)\Delta t}^{(n)} - x_{k\Delta t}^{(n)} + \nabla \Psi_{\hat{\theta}}(x_{k\Delta t}^{(n)}) \Delta t \right\|_2^2 \\ 0 &= dNT - \frac{1}{\sigma^2 \Delta t} \ell(\hat{\theta}) \\ \sigma^2 &= \frac{1}{dNT \Delta t} \ell(\hat{\theta}) \end{aligned}$$

F Potentials

Our experiments consider the following potentials for simulating gradient-flow SDEs. In particular, these are the potentials from [Terpin et al. \[2024\]](#), which admit a valid stationary Gibbs distribution $p_{\text{eq}} = \frac{1}{Z} \exp\left(-\frac{\Psi}{2\sigma^2}\right)$.

$$\text{Bohachevsky} \quad \Psi(x) = 10(x_1^2 + 2x_2^2 - 0.3 \cos(3\pi x_1) - 0.4 \cos(4\pi x_2)) \quad (36)$$

$$\text{Oakley–O’Hagan} \quad \Psi(x) = 5 \sum_{i=1}^2 (\sin(x_i) + \cos(x_i) + x_i^2 + x_i) \quad (37)$$

$$\text{Quadratic} \quad \Psi(x) = 5 \|x\|^2 \quad (38)$$

$$\text{Styblinski–Tang} \quad \Psi(x) = \frac{1}{2} \sum_{i=1}^2 (x_i^4 - 16x_i^2 + 5x_i) \quad (39)$$

$$\text{Wavy plateau} \quad \Psi(x) = \sum_{i=1}^2 (\cos(\pi x_i) + \frac{1}{2}x_i^4 - 3x_i^2 + 1) \quad (40)$$

Each of these potentials is smoothly differentiable and hence Lipschitz. In order to satisfy the linear growth condition, $\|\nabla \Psi(x)\| \leq K(1 + \|x\|)$, assumed for the existence of strong solutions to the SDE (1), we can multiply potentials by a smooth cutoff function, which is 1 in $\|x\| \leq M$ and 0 in $\|x\| > 2M$. Choosing $M = 100$ for our experiments do not alter data generation compared to the raw setting.

G Additional experiments

Software and hardware details. The code in this paper were adapted from two public code repositories (**APPEX**: <https://github.com/guanton/APPEX> and **JKonet***: <https://github.com/antonioterpin/jkonet-star>). All computations are performed on a 2024 MacBook Pro with 16GB RAM and an Apple M4 chip. The code was adapted to design the experiments, visualize the data, and interpret the results. It is available in the supplementary material.

G.1 Experimental setup

Since the objective of our main experiments was to evaluate the inferential power of different Schrodinger bridge methods, we considered the methods **WOT**, **SBIRR**, and **nn-APPEX** (ours), and we simulated data from a range of population dynamics for each SDE, by randomizing the initial distribution over Gaussian mixtures. We perform two additional experiments, such that we use the same experimental setup, but consider two particular initial distributions: the uniform distribution over the region of interest $[-4, 4]^2$ and the stationary Gibbs distribution p_{eq} . In order to sample from the Gibbs distributions $\frac{1}{Z} \exp\left(-\frac{2\Psi(x)}{\sigma^2}\right)$, we generate trajectories from $p_0 = \text{Unif}([-4, 4]^2)$ and run 200 steps of the SDE with step size $\Delta t = 0.01$. Indeed, each of the potentials (36)-(40) satisfies the Poincaré inequality, which ensures that marginals converge exponentially quickly to the stationary Gibbs distribution [[Pavliotis, 2014](#), Theorem 4.4].

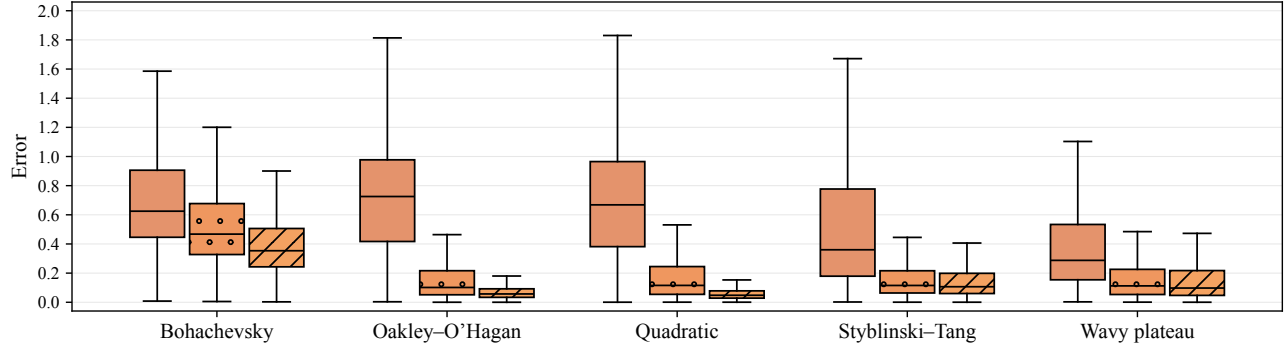
We also perform additional experiments comparing our method, **nn-APPEX**, against the state-of-the-art variational method, **JKOnet*** [Terpin et al., 2024]. We implement **JKOnet*** with default hyperparameters, and use 100 training epochs, noting rapid convergence of the objective. We verified in a separate experiment that running with 10000 epochs did not meaningfully change performance. The experimental setting is the main setting over random GMM initializations, in order to test on different population dynamics. Since **JKOnet*** also jointly estimates drift and diffusion for the gradient-flow SDE (1), we additionally report diffusivity MAE for this experiment.

G.2 Results

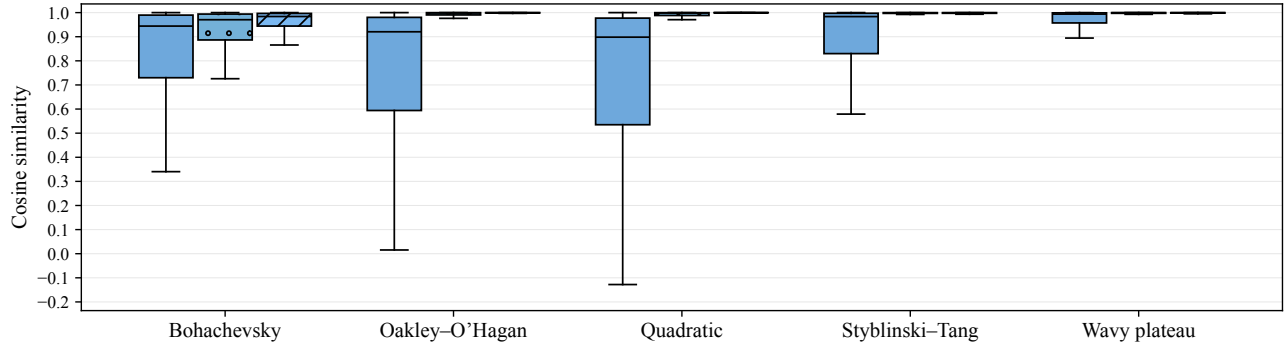
The uniform initial distribution $p_0 \sim \text{Unif}[-4, 4]^2$ represents an idealized benchmark [Terpin et al., 2024] while the stationary distribution $p_0 \sim p_{\text{eq}}$ represents the non-identifiable setting. Results comparing the three SB methods, **WOT**, **SBIRR**, and **nn-APPEX**, are summarized for the uniform initialization in Fig. 4 and for the non-identifiable stationary initialization in Fig. 5.

We also present results from our main experimental setting (random GMM initializations), which compare our method **nn-APPEX** against **JKOnet*** in Fig. 6. The results show that **nn-APPEX** accurately infers both the drift and diffusivity to high precision for all SDEs, and outperforms **JKOnet*** except for the diffusivity estimate of the Bohachevsky potential. We note that the Bohachevsky potential is particularly difficult to estimate, as it has the highest magnitude, and converges to its Gibbs distribution p_{eq} at a much faster rate than the other SDEs, all while exhibiting highly periodic and nonlinear dependencies. For this reason, the MLE diffusion estimate by **nn-APPEX** likely achieves biased estimates, since the adjusted quadratic variation (17) is impacted by poor drift estimation. This is also consistent with previous results [Terpin et al., 2024], which showed that the Bohachevsky potential is particularly difficult to estimate in dimension $d = 2$.

(a) Absolute drift error (normalized by true magnitude)



(b) Cosine similarity



WOT



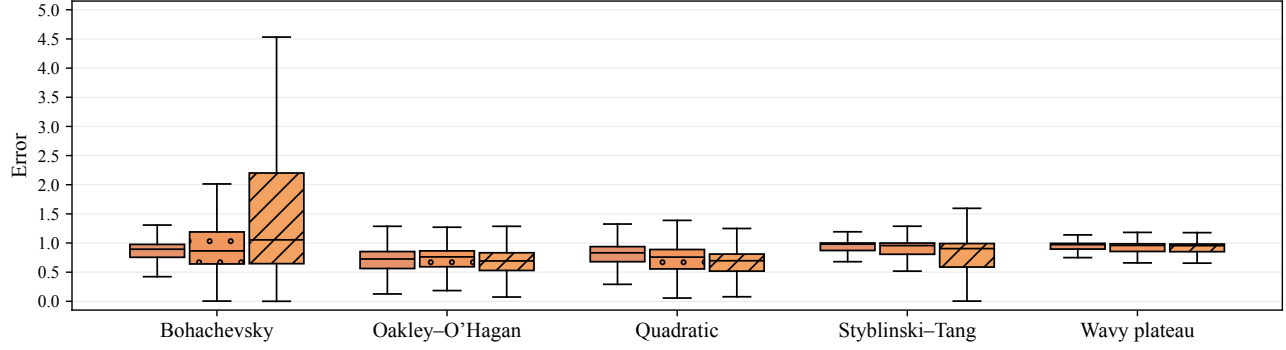
SBIRR



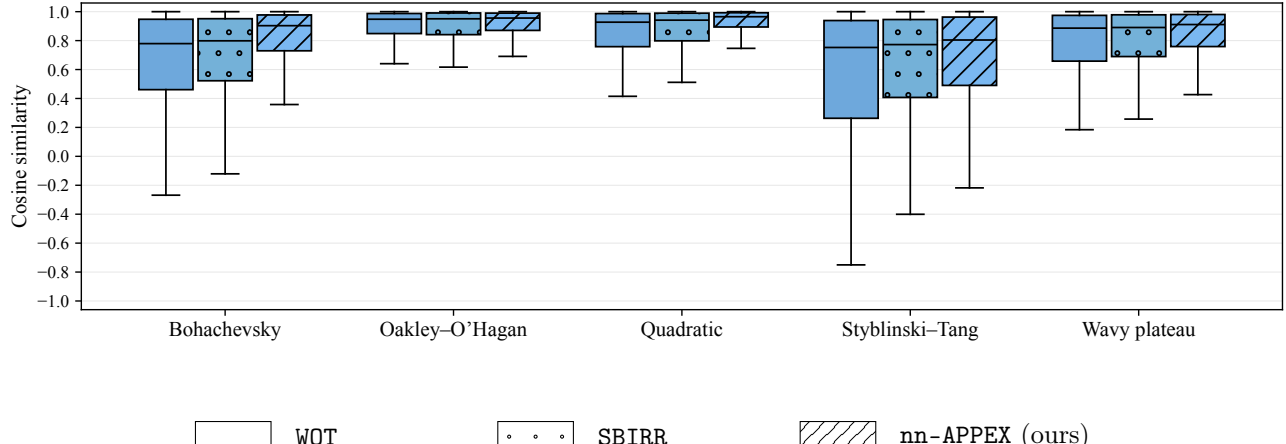
nn-APPEX (ours)

Figure 4: The ability of different Schrödinger Bridge methods to infer the gradient-flow drift is evaluated across five potentials using (a) normalized absolute error and (b) cosine similarity. Here, methods observe three marginals with a uniform initial distribution in the region of interest, i.e. $p_0 \sim \text{Unif}[-4, 4]^2$. Box-and-whisker plots over 10 seeds show nn-APPEX performs best across all potentials.

(a) Absolute drift error (normalized by true magnitude)



(b) Cosine similarity



WOT



SBIRR



nn-APPEX (ours)

Figure 5: The ability of different Schrödinger Bridge methods to infer the gradient-flow drift is evaluated across five potentials using (a) normalized absolute error (lower is better) and (b) cosine similarity (higher is better). Methods observe three marginals with the initial distribution equal to the SDE's stationary Gibbs distribution, $p_0 \sim p_{\text{eq}}$. Aggregated box-and-whisker plots over 10 seeds show that all methods perform similarly poorly, corroborating Theorem 4.1: the true gradient-flow drift is not identifiable without knowing the diffusivity.

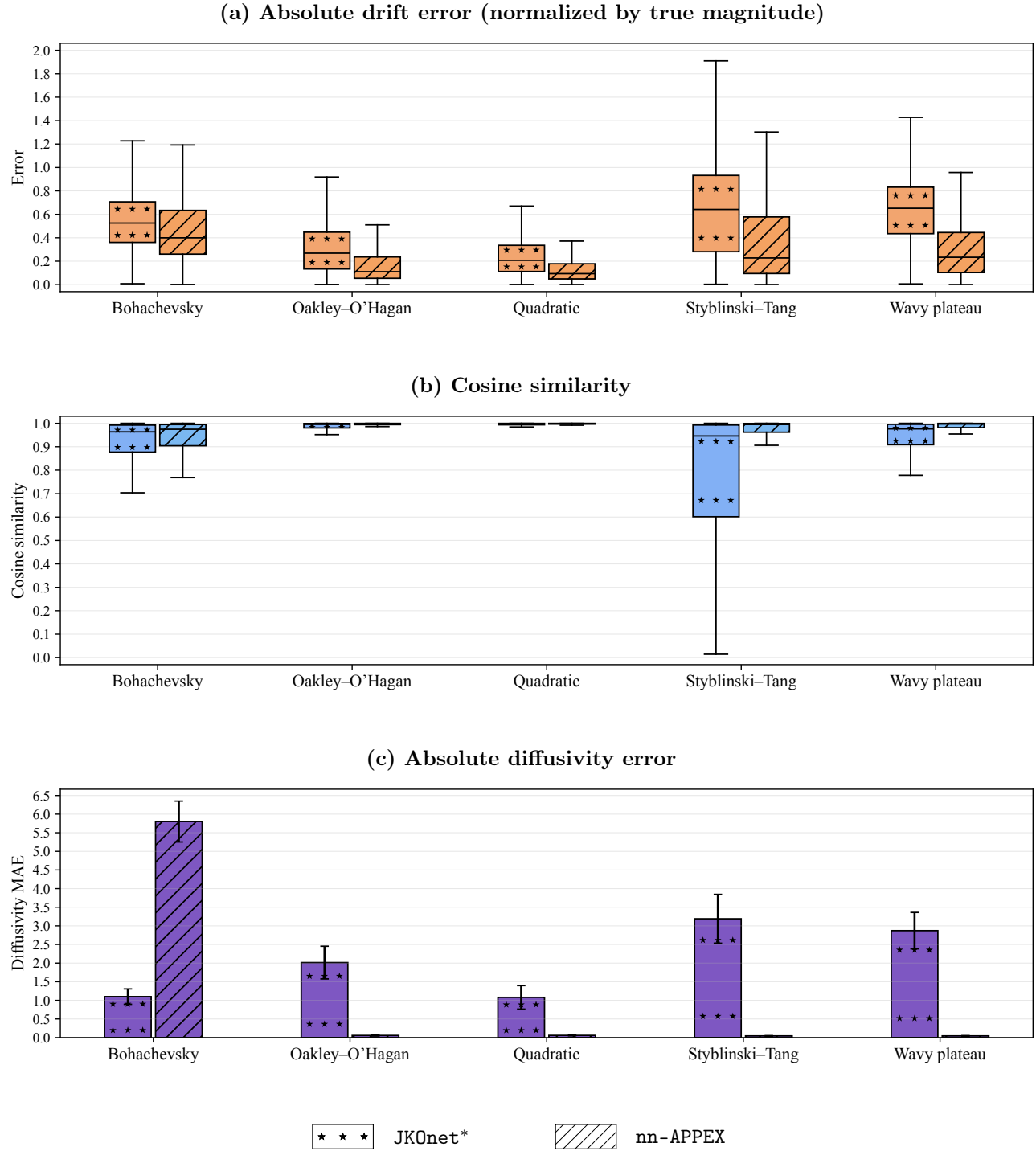


Figure 6: The ability of the variational method **JKOnet*** and **nn-APPEX** (ours) to infer the gradient-flow drift is evaluated across five potentials using (a) normalized absolute error (lower is better) and (b) cosine similarity (higher is better), and their ability to infer the diffusivity is evaluated using (c) absolute error (lower is better). Both methods are given samples from three distinct marginals, such that the initial distribution is a Gaussian mixture model with randomly initialized components. The plots aggregated from 10 seeds show that our method, **nn-APPEX** achieve better estimation of the drift and diffusion in this setting, except for the Bohachevsky potential.